British Journal of Pharmacology

DOI:10.1111/j.1476-5381.2011.01730.x
www.brjpharmacol.org

RESEARCH PAPER

Potassium and ANO1/ TMEM16A chloride channel profiles distinguish atypical and typical smooth muscle cells from interstitial cells in the mouse renal pelvis

Correspondence
Dr RJ Lang, Department of Physiology, Monash University, Clayton, Vic. 3800, Australia.
E-mail:
rick.lang@med.monash.edu.au

Keywords
pyeloureteric peristalsis; upper urinary tract; smooth muscle; calcium signalling; pacemakers

Received
4 November 2010
Revised
25 September 2011
Accepted
1 October 2011

Javed Iqbal[1], Mary A Tonta[1], Retsu Mitsui[3], Qun Li[1], Michelle Kett[1], Jinhua Li[2], Helena C Parkington[1], Hikaru Hashitani[3] and Richard J Lang[1]

Departments of [1]Physiology and [2]Anatomy & Development Biology, School of Biomedical Sciences, Monash University, Clayton, Victoria, Australia, and [3]Department of Cell Physiology, Nagoya City University, Graduate School of Medical Sciences, Nagoya, Japan

BACKGROUND AND PURPOSE

Although atypical smooth muscle cells (SMCs) in the proximal renal pelvis are thought to generate the pacemaker signals that drive pyeloureteric peristalsis, their location and electrical properties remain obscure.

EXPERIMENTAL APPROACH

Standard patch clamp, intracellular microelectrode and immunohistochemistry techniques were used. To unequivocally identify SMCs, transgenic mice with enhanced yellow fluorescent protein (eYFP) expressed in cells containing α-smooth muscle actin (α-SMA) were sometimes used.

KEY RESULTS

Atypical SMCs were distinguished from typical SMCs by the absence of both a transient 4-aminopyridine-sensitive K^+ current (I_{KA}) and spontaneous transient outward currents (STOCs) upon the opening of large-conductance Ca^{2+}-activated K^+ (BK) channels. Many typical SMCs displayed a slowly activating, slowly decaying Cl^- current blocked by niflumic acid (NFA). Immunostaining for $K_V4.3$ and ANO1/ TMEM16A Cl^- channel subunits co-localized with α-SMA immunoreactive product predominately in the distal renal pelvis. Atypical SMCs fired spontaneous inward currents that were either selective for Cl^- and blocked by NFA, or cation-selective and blocked by La^{3+}. α-SMA^- interstitial cells (ICs) were distinguished by the presence of a Xe991-sensitive K_V7 current, BK channel STOCs and Cl^- selective, NFA-sensitive spontaneous transient inward currents (STICs). Intense ANO1/ TMEM16A and $K_V7.5$ immunostaining was present in Kit^- α-SMA^- ICs in the suburothelial and adventitial regions of the renal pelvis.

CONCLUSIONS AND IMPLICATIONS

We conclude that $K_V4.3^+$ α-SMA^+ SMCs are typical SMCs that facilitate muscle wall contraction, that ANO1/ TMEM16A and $K_V7.5$ immunoreactivity may be selective markers of Kit^- ICs and that atypical SMCs which discharge spontaneous inward currents are the pelviureteric pacemakers.

Abbreviations

$[Ca^{2+}]_I$, intracellular concentration of Ca^{2+}; α-SMA, α-smooth muscle actin; BK channel, large conductance calcium-activated potassium channel; CaCCs, Ca^{2+}-activated Cl^- channels; eYFP, enhanced yellow fluorescent protein; ICs, interstitial cells; I_{KA}, 4-aminopyridine-sensitive K^+ current; LICs, large inward currents; MCA, meclofenamic acid; NFA, niflumic acid; PSS, physiological salt solution; SMCs, smooth muscle cells; STICs, spontaneous transient inward currents; STOCs, spontaneous transient outward currents; TEA, tetraethylammonium

Introduction

Movement of urine from the kidney through the ureter to the bladder occurs via the means of propagating contractions (pyeloureteric peristalsis), which originate spontaneously within the most proximal regions of the renal pelvis (Weiss *et al.*, 1967; Golenhofen and Hannappel, 1973). In most mammals, urine is expressed from a single papilla into a funnel-shaped calyx or renal pelvis consisting of an impermeable urothelium and a muscle wall of 'typical' smooth muscle cell (SMCs). In the human and pig, the kidney is multipapillate so that several calyces fuse to form a separate renal pelvis (Dixon and Gosling, 1973; 1982; Gosling and Dixon, 1974). Over the last 30 years, evidence has been increasing that the pacemaker cells driving pyeloureteric peristalsis are 'atypical' SMCs, which form a relatively-sparse outer layer in uni-calyceal kidneys, or an inner layer in multi-calyceal kidneys, that wraps around the most proximal regions of the papilla base (Dixon and Gosling, 1973; 1982; Gosling and Dixon, 1974; Lang *et al.*, 1998; Klemm *et al.*, 1999).

In excised preparations of renal pelvis (Klemm *et al.*, 1999; Lang *et al.*, 2001; Tsuchida and Suzuki, 1992), in which the contraction has been arrested with the L-type Ca^{2+} channel blocker nifedipine, spontaneous transient depolarizations (STDs) are recorded in atypical SMCs and thought to arise from the opening of cation-selective channels activated by transient increases in the intracellular concentration of Ca^{2+} ($[Ca^{2+}]_i$), as Ca^{2+} is released from internal stores (Lang *et al.*, 2007b; 2010). In the mouse, these Ca^{2+} transients take the form of distinct slow velocity intercellular Ca^{2+} waves that seldom propagate into neighbouring cells (Lang *et al.*, 2007a). Synchronization of STDs in neighbouring atypical SMCs in the absence of nifedipine into a pacemaker signal that evokes action potential discharge and contraction in the typical SMC layer is presently thought to involve Ca^{2+} entry through L-type Ca^{2+} channels and the uptake and accelerated release of Ca^{2+} from both IP_3- and ryanodine-receptor coupled Ca^{2+} stores (Lang *et al.*, 2007b; 2010; Berridge, 2008), intimately dependent on the movement of Ca^{2+} through neighbouring mitochondria (Hashitani *et al.*, 2009).

In this study, we have recorded the electrical activity in single SMCs and interstitial cells (ICs) isolated after enzymatic dispersal of the mouse renal pelvis using standard whole-cell (at 22°C) or nystatin perforated-patch (at 37°C) voltage clamp techniques. Antibodies raised against the likely subunits of the K^+ and Cl^- channels identified were also applied to coronal sections of mouse kidney to determine the location of these cells *in situ*. In some experiments, we have used a transgenic mouse that has an enhanced yellow fluorescent protein (eYFP) coupled to the promoter for the gene controlling α-smooth muscle actin (α-SMA) expression (Li *et al.*, 2009) and established that two populations of eYFP-α-SMA^+ cells could be distinguished on the basis of their ion channel profiles, while α-SMA^- ICs were distinguished by the presence of a transient K^+ current that was blocked by Xe991, a blocker of K_V7 channel currents.

We have concluded that typical SMCs possess a membrane ion channel profile similar to that reported in SMCs from mouse ureteropelvic junction (Lang *et al.*, 2007c) and guinea-pig (Lang, 1989) or rat (Smith *et al.*, 2002) ureter. Atypical SMCs have a unique compliment of membrane channels and discharge spontaneous inward 'pacemaker' currents. Finally, ANO1/ TMEM16A Cl^- channel and $K_V7.5$ channel subunit immunoreactivity may prove to be useful markers of IC distribution and remodelling in the renal pelvis, particularly in pathological conditions such as ureteric obstruction or infection.

Methods

Conventional Swiss outbred or Balb/C mice of either sex and female eYFP–α-SMA transgenic mice (6–10 weeks of age) were killed by cervical dislocation and exsanguination; their kidneys and attached ureters were removed using procedures approved by the School of Biomedical Sciences Animal Ethics Committee at Monash University. eYFP-α-SMA^+ mice were kindly provided by Dr James Lessard (Cincinnati Children Hospital Medical Centre, Cincinnati, OH, USA) (Li *et al.*, 2009). Rat kidneys were obtained from Sprague–Dawley rats deeply anaesthetized with isoflurane inhalation anaesthetic (4% Baxter Health Care Ltd., NSW, Australia).

Immunohistochemistry

Kidneys were either perfused transcardially with 0.1 M PBS followed by 50 mL of 4% paraformaldehyde in 0.1 M PBS or excised, cut into 2–6 mm transverse sections and fixed in ice-cold acetone for 30 min, sometimes after a 30 min wash in 2% paraformaldehyde (in 0.1 M PBS). Specimens were then washed in 0.1 M PBS for 10 min and then placed in 30% sucrose in PBS overnight before being frozen on dry ice and stored at –20°C. Coronal sections (10 µm) were cut and mounted onto pre-coated slides (Superfrost; Thermo Scientific, Victoria, Australia), air-dried for 30 min at room temp and stored at –20°C until processed for immunohistochemistry. Positive control tissues for channel subunit and Kit staining included sections obtained from the proximal colon and brains fixed in 4% paraformaldehyde in 0.1 M PBS. Observations were made from 5 to 10 coronal sections cut from both kidneys obtained from three to eight animals.

Slide-mounted sections were brought to room temperature and submerged in cold acetone for 10 min and washed in 0.05 M PBS. After being blocked (5% normal goat serum, 5% normal horse serum, 1% BSA and 0.3% Triton X-100 in 0.1 M PB) for 30 min, sections were incubated with either rabbit polyclonal or monoclonal antibodies or a cocktail of antibodies for 48 h at 4°C. Sections were incubated with anti-$K_V4.3$ (H-225, 1:500; Sc: 28634, Santa Cruz Biotechnology, Inc., Santa Cruz, CA, USA), anti- $K_V7.5$ (KCNQ5) (ab84819; 1:500; Abcam Plc, Cambridge, UK), ANO1/ TMEM16A (ab53212; 1:500; Abcam), anti-α-SMA (1:2500; Sigma Aldrich, Castle Hill, Australia), anti-Kit (CD117) (AK2 1:500; Calbiochem, Kilsyth, Australia) or PGP9.5. After being washed, sections were then incubated with goat anti rabbit Alexa 546 (red, 1:500; Molecular Probes, Eugene, OR, USA) or goat anti mouse Alexa 488 (green, 1:500; Molecular Probes) in 0.1 M PB for 1 h and washed. Sections were washed again in 0.1 M PBS and coverslipped with anti-fade medium (Dako Corp., Carpinteria, CA, USA). Sections were viewed with a Zeiss fluorescent microscope, and images were captured using Axiovision (Carl Zeiss, North Ryde, Australia) computer software.

Intracellular microelectrode recordings

Renal pelvis preparations were pinned onto a Sylgard plate (silicone elastomer, Dow Corning Corporation, Midland, MI, USA) situated in the bottom of the recording chamber (volume, approximately 1 mL). The preparations were superfused with warmed (36°C) bicarbonate-buffered physiological salt solution (bPSS) at a constant flow rate (2 mL·min^{-1}) and were allowed to equilibrate for 30 min. Individual typical SMCs in the renal pelvis wall were impaled with glass capillary microelectrodes with tip resistance of 100–200 MΩ, when filled with 0.5 M KCl. Membrane potential changes were recorded using a high-input impedance amplifier (Axoclamp-2B, Axon Instruments, Inc., Foster City, CA, USA) and digitized, after low-pass filtering (cut-off frequency, 10 kHz), using a Digidata 1322 interface (Axon Instruments, Inc.) and stored on a personal computer for later analysis.

Collagenase dispersal of cells from the renal pelvis

Single cells of the renal pelvis from conventional or eYFP-α-SMA$^+$ mice were dispersed using collagenase as previously described (Lang *et al.*, 2007c) using a low-Ca^{2+} HEPES-buffered PSS (hPSS) containing collagenase type I (2 mg·mL^{-1} Worthington), protease type XXIV (60 μg·mL^{-1}), trypsin inhibitor type II (1 mg·mL^{-1}) and bovine serum albumin (1 mg·mL^{-1}; all from Sigma Aldrich). Cells released by gentle stirring in enzyme-free low Ca^{2+} PSS were stored at 4°C until experimentation. Cells in suspension were allowed to settle onto the bottom of a recording chamber, mounted on an inverted microscope and perfused with hPSS containing 1.5 mM Ca^{2+}. Recordings were made at either 22°C or 37°C.

Single-cell recordings

Both whole-cell (at 22°C) and nystatin perforated-patch (at 37°C) voltage clamp techniques were used. Nystatin (Sigma) was dissolved in dimethyl sulphoxide (stock concentration 27 mM) and added to the pipette solution at 2 μL·mL^{-1}. Depolarizing voltage steps (200 ms duration) were applied from a holding potential of −60 mV in increments of 10 mV between −70 and +60 mV after a 800 ms conditioning step to −90 mV. When direct comparisons between cells were required, current–voltage (*I–V*) plots of the peak (I_{Peak}) and steady-state (I_{ss}) current recorded at the end of each depolarizing step were normalized for cell capacitance, averaged and plotted against the membrane potential that was corrected for the junction potential arising from the differing pipette solutions used (Lang *et al.*, 2007c). In some experiments, ramped depolarizations (from −114 to +64 mV over 500 ms) were applied from a holding potential of −60 mV.

Solutions and drugs

During the intracellular microelectrode studies, the bPSS contained (in mM): NaCl 120, KCl 4.7, $CaCl_2$ 2.5, $MgCl_2$ 1.2, $NaHCO_3$ 15.5, KH_2PO_4 1.2 and glucose 15. The pH of this PSS was 7.2 when bubbled with 95% O_2 and 5% CO_2. The hPSS for the patch clamp experiments contained (mM): NaCl 126, KCl 6, sodium N-2-hydroxyethylpiperazine-N′-2-ethansulphonic acid (Na-HEPES) 10, $MgCl_2$ 1, D-glucose 10, and $CaCl_2$ 50 μM when digesting cells and 1.5 mM during experimentation. In some experiments, the total extracellular Na^+ concentration was reduced to 30 mM using an equimolar replacement of NaCl with tetraethylammonium chloride (115 mM TEACl) as the impermeant ion. The pH of the solution was adjusted to 7.2 with 5 M NaOH. The pipette solution contained (mM): KCl 130, CsCl 130 or a KCl 15 : Kgluconate 115 mixture; Na-HEPES 10; EGTA 0.3; $MgCl_2$ 1 and nystatin; pH was set at 7.4 with 5 M KOH. During the whole-cell patch clamp experiments, this solution also contained 1 mM ATP.

Data analysis

Means ± SEM are presented, with *N* denoting the number of animals and *n* the number of cells. Student's paired or unpaired *t*-tests were used for tests of significance; $P < 0.05$ was accepted as statistically significant (Lang *et al.*, 2007c).

All channel nomenclature conform to BJP's *Guide to Receptors and Channels* (GRAC), 5th edition (Alexander *et al.*, 2011).

Results

SMCs within the renal pelvis wall

Peristaltic pyeloureteric contractile activity in eYFP-α-SMA$^+$ transgenic mice was indistinguishable from that observed in conventional Swiss or Blab/C mice, male or female, and could be observed in intact tubular preparations (Figure S1Ai–iii and Video S1) or in whole mount preparations pinned flat in an organ bath (Figure S1C, Video S2). Individual spindle-shaped eYFP-α-SMA$^+$ SMCs in micrographs of whole-mount preparations, taken under identical illumination parameters, appeared longer and brighter with distance from the papilla (Figure S1Ci–ii). In coronal sections of renal pelvis, eYFP–α-SMA$^+$ SMCs are clearly more tightly packed in the muscle coat, which gradually thickened with distance from the papilla–pelvis border (Figure S1Di–iii). In each kidney, there was at least one section that displayed a cluster of lightly fluorescent short eYFP-α-SMA$^+$ SMCs (Figure S1Diii) in the very most proximal regions of the renal pelvis adjacent to the base of the papilla.

Electrical recordings from α-SMA-eYFP$^+$ SMCs

Upon illumination with blue (482 nm) fluorescent light, the eYFP-α-SMA$^+$ SMCs dispersed from the renal pelvis were readily distinguished from other urothelial cells and ICs. eYFP-α-SMA$^+$ cells were either spindle-shaped (Figure 1Ci–ii) or displaying some degree of contraction (Figure 1Ai–ii). When these eYFP-α-SMA$^+$ cells were examined electrophysiologically, using the perforated patch whole-cell voltage clamp technique (at 37°C) and a two-step protocol for evoking the opening and closing of voltage-operated membrane channels, they were readily divided into two distinct populations of 'typical' and 'atypical' SMCs identified, respectively, on the basis of the presence (Figure 1B; $n = 7$ cells from $N = 4$ animals) or absence (Figure 1D; $n = 8$ $N = 4$) of a voltage-operated transient K^+ current, which inactivated during a conditioning step to −54 mV.

Electrical properties of typical SMCs

Whole-cell voltage clamp recordings (at 22°C) of SMCs from the distal renal pelvis (ureteropelvic junction) using KCl

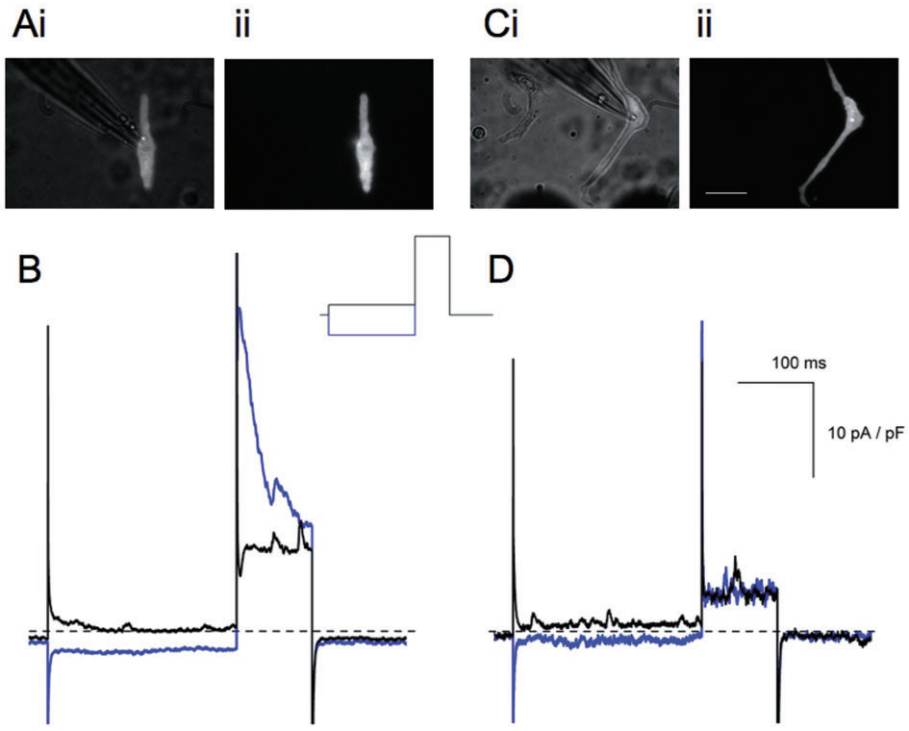

Figure 1

Recording from single SMCs isolated from α-SMA-eYFP transgenic mice. Single α-SMA-eYFP$^+$ SMCs were readily visible when exposed to blue (482 nm) light in the presence (Ai, Ci) or absence (Aii, Cii) of bright field illumination. The electrical properties of α-SMA-eYFP$^+$ SMCs cells fell into two distinct types based on the presence (B) or absence (D) of a transient 'A-type' K^+ current (I_{KA}). Membrane currents were recorded in response to a depolarizing voltage step to 4 mV after a conditioning step to either –94 (blue trace) or –54 (black trace), from a holding potential of –74 mV (see insert) using the perforated-patch whole cell voltage clamp (at 37°C) and Kgluconate : KCl-filled pipettes. Dashed line represents zero current; calibration bars apply to both (B) and (D).

(130 mM)-filled pipettes have previously established the presence of an 'A-type' transient K^+ current (I_{KA}) that activated rapidly (within 5–10 ms) at potentials positive to –60 mV and then decayed over 200–300 ms (Lang *et al.*, 2007c). This I_{KA} was generally followed by a more slowly developing and decaying K^+ current that was attributed to the opening and closing of TEA/ iberiotoxin-sensitive BK channels (Figure 2Ai). However, in the present experiments when the nystatin perforated-patch technique (at 37°C) was applied to SMCs isolated from conventional or eYFP-α-SMA$^+$ mice and the pipette contained KCl (n = 8 cells from N = 6 animals; Figure 2Aii) or the Kgluconate (115 mM) : KCl (15 mM) mixture (n = 21 cells from N = 14 animals; Figure 2Aiii and Bi), this second TEA-sensitive K^+ current tended to be relatively small (Figure 2Aii and Bii), or manifest only as STOCs (Figure 2Aiii). These STOCs were small at a holding potential of –64 mV but increased in amplitude and frequency at potentials more positive (Figure 2Aiii).

Figure 2Bi–ii shows that I_{KA} was readily blocked by 2 mM 4-aminopyridine (4-AP), the selective blocker of 'A-type' K^+ currents generated by K_V4.x or K_V1.4 α-subunits of the superfamily of six transmembrane domain K^+ channels (Figure 2Bi–ii and C) (Alexander *et al.*, 2011). The membrane currents remaining in the presence of 4-AP were readily reduced upon blockade of BK channels with 2 mM TEA (Figure 2Bii–iii). The mean *I–V* plots of I_{Peak} of I_{KA} (Figure 2C) and I_{SS} (Figure 2C) averaged from five typical SMCs recorded with Kgluconate : KCl-filled pipettes (at 37°C) in the absence or presence of 2 mM 4-AP and 2 mM TEA are plotted in Figure 2C. These I_{Peak} values were then used to calculate the mean normalized activation data for I_{KA} (n = 5; Figure 2D), which when fitted with a Boltzmann equation gave a voltage of half-maximal activation ($V_{0.5}$) of –9.4 mV and slope value (K) of 16.3 mV.

The steady-state inactivation characteristics of I_{KA} were also examined in four cells bathed in 1 μM nifedipine and 2 mM TEA using a twin-step protocol. I_{KA} (at +4 mV) decreased in amplitude as conditioning steps (between –114 and –24 mV for 10 s) were made to increasingly more positive potentials. Normalized I_{KA} values (I/Imax) when averaged, plotted against the conditioning potential (Figure 4D) and fitted with a Boltzmann equation gave a $V_{0.5}$ of –63.7 mV, K of 11.3 mV and a non-inactivating component of 0.05. The red plots in Figure 2D represent the equivalent activation and inactivation characteristics of I_{KA} previously obtained in typical SMCs at 22°C using KCl-filled pipettes (Lang *et al.*, 2007c).

It is apparent that experimentation at room temperature and the dialysis of cells using whole-cell voltage clamp techniques has a considerable influence on the voltage-dependence of I_{KA}, shifting its inactivation curve some 20 mV in the negative direction, as well as slowing the time course of

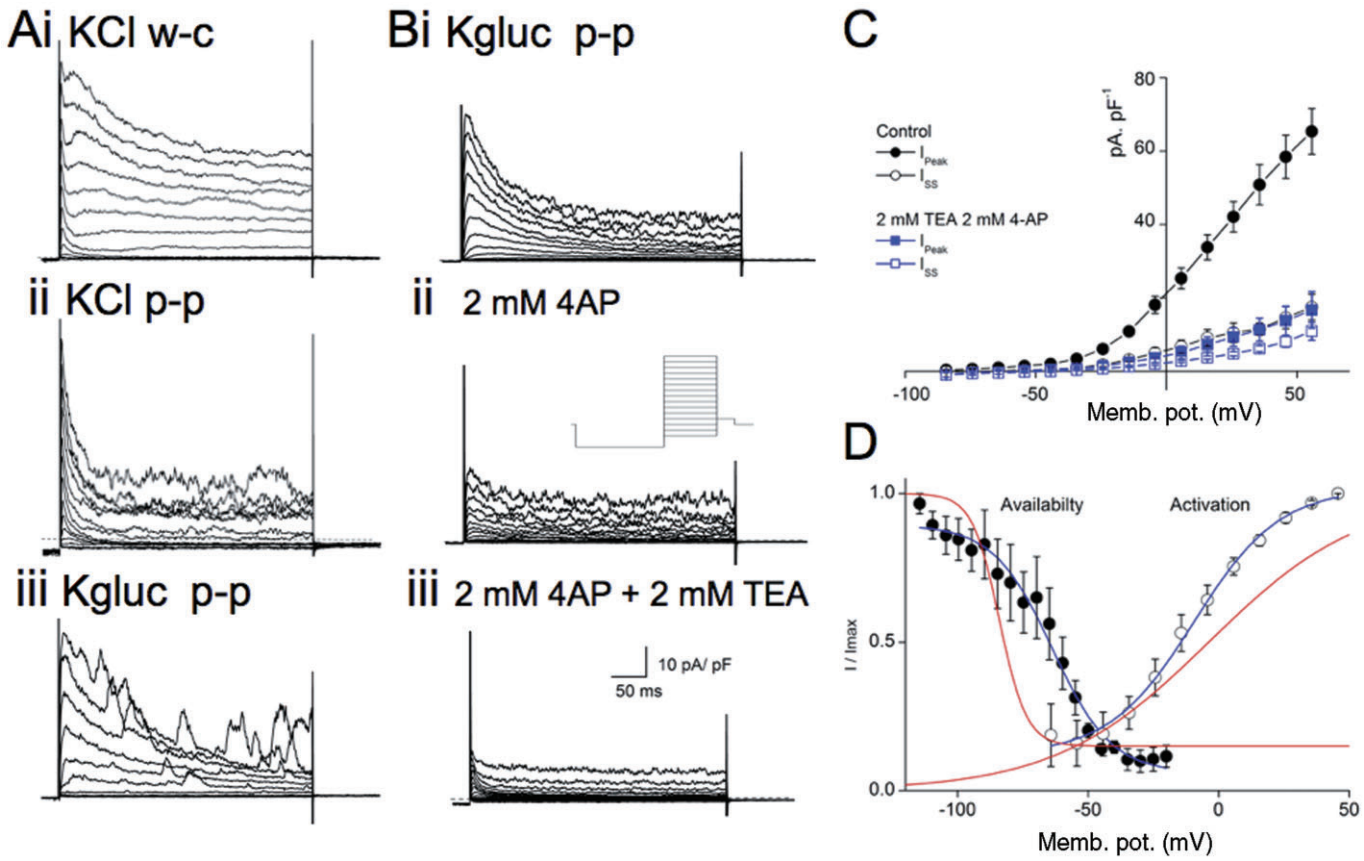

Figure 2

Electrical properties of typical SMCs. (A) Comparison of the membrane currents recorded in typical SMCs recorded using KCl (130 mM)-filled pipettes and either the whole cell (Ai, KCl w-c at 22–24°C) or nystatin perforated patch (Aii, KCl p-p at 37°C) voltage clamp technique (Aiii). (Bi) Membrane currents in typical SMCs recorded with Kgluconate (115 mM) : KCl (15 mM)-filled pipettes using nystatin perforated patch voltage clamp (Kgluc p-p at 37°C). Dashed line represents zero current; calibration bars apply to all panels. Note the more rapid decay of the outward currents and the presence of spontaneous outward currents (STOCs) at 37°C. (Bi–ii) The peak amplitude (I_{Peak}) of the outward current (I_{KA}) recorded in cells bathed in 1 μM nifedipine was blocked by a 10 min exposure to 2 mM 4-AP; the remaining steady-state current (I_{SS}) was blocked by 2 mM tetraethylammonium (TEA), blocker of BK channels (Biii). (C) I_{Peak} and I_{SS} of I_{KA} from five typical SMCs in the absence and after 10 min exposure to 2 mM TEA + 2 mM 4-AP were normalized for cell capacitance, averaged and plotted against potential. The activation range of I_{KA} was determined by first dividing I_{Peak} of the individual I_{KA} (C) at various potentials by their driving force (V+81.7 mV), assuming a reversal potential for a K^+ conductance of –81 mV. Normalized g_{KA} were then obtained by expressing values as a fraction of their maxima (g_{KA}/ g_{KAmax}). Mean data (D) were plotted against potential and fitted with a Boltzmann function to give a $V_{0.5}$ of –9.4 mV and slope factor of 16.3 mV. Steady-state inactivation characteristics of I_{KA} were examined using a two-step depolarizing protocol in which cells were held at –64 mV and then stepped to conditioning potentials every 5 mV between –120 and –10 mV (for 10 s) before a test step (200 ms duration) to +16 mV was applied. The availability plot of I_{KA} (n = 4) was obtained by normalizing I_{Peak} at +16 mV after each conditioning potential as a fraction of their maxima (I/ I_{max}) and plotting the average (D) of these relative amplitudes against the conditioning potential (V). This plot was fitted with a sigmoidal Boltzmann equation with $V_{0.5}$ of –64.3 mV and slope factor of 11.2 mV. The other red plots indicate the activation and availability curves previously obtained when KCl-filled pipettes and the whole cell voltage clamp technique was used (at 22–24°C) (Lang *et al.*, 2007c).

BK channel currents (cf. Figure 2Ai and Bi). Both phenomena could well be attributed to the differing Ca^{2+} buffering conditions within the cell in the two recording modes.

Cl^- currents in typical SMCs

At a holding potential –74 mV, typical SMCs recorded with Kgluconate : KCl-filled pipettes (at 37°C) often displayed small-amplitude STOCs, which grew in amplitude with membrane depolarization (Figure 2Aiii). These typical SMCs also sometimes displayed a small inward tail current (at –64 mV) upon repolarization from positive potentials (Figure 3Ai), as well as small-amplitude spontaneous transient inward currents (STICs) at –74 mV. In the SMC illustrated in Figure 3Aii, the mean amplitude of 30 of these STICs was 7.32 ± 1.02 pA, their half width was 164.8 ± 45.1 ms, their time to peak amplitude 783.5 ± 75.9 ms (n = 30), while their frequency of discharge was 10 min^{-1}.

In typical SMCs, voltage clamped with KCl-filled pipettes and the perforated patch technique (at 37°C), membrane depolarization often (n = 12 of 48 cells examined) evoked a slowly developing current that was inward between –44 and –24 mV and outward at potentials more positive (Figure 3Bi

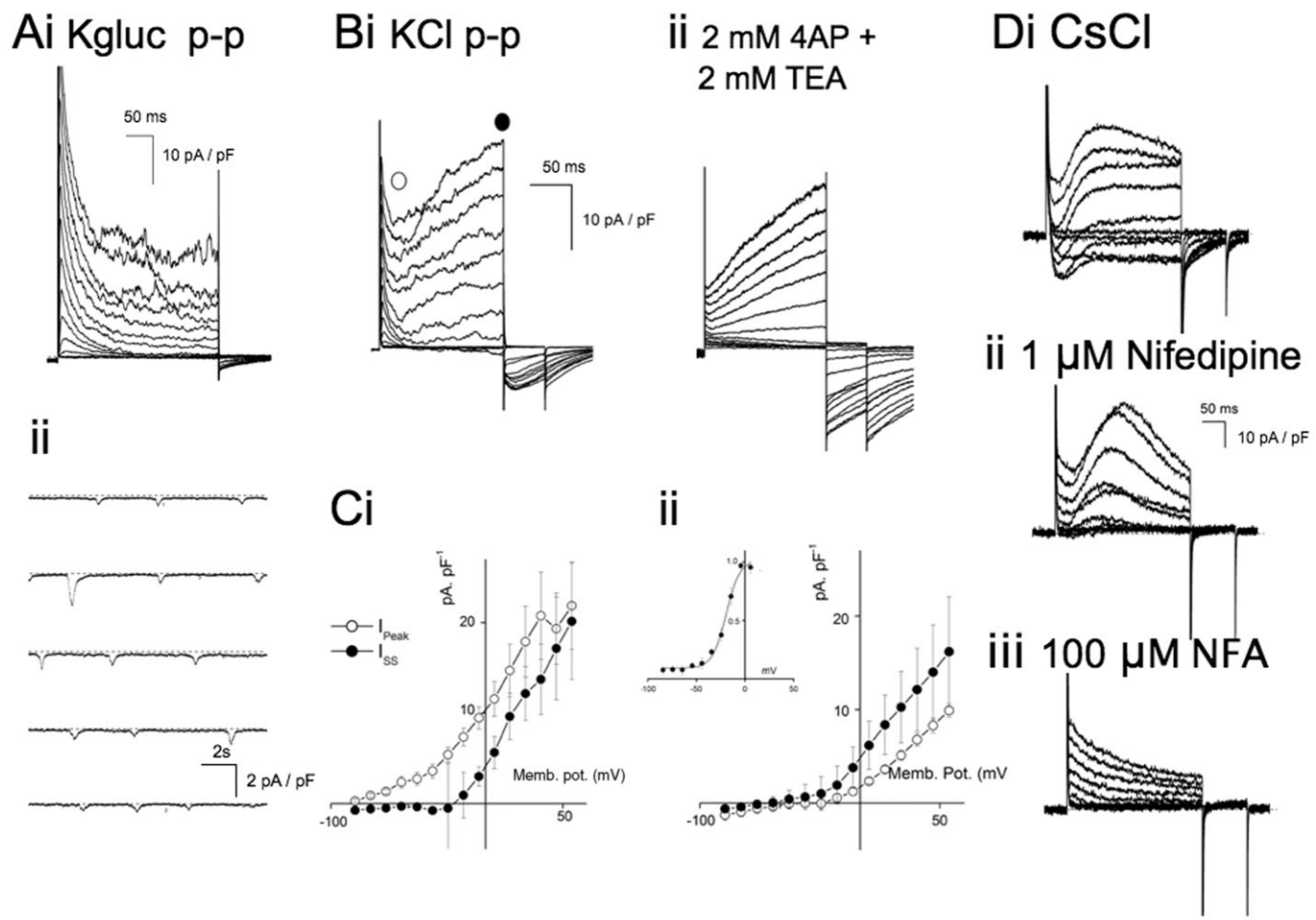

Figure 3

Cl^- currents in typical SMCs. Some typical SMCs recorded with Kgluconate : KCl-filled (Ai) or KCl-filled (Bi) pipettes and the nystatin perforated patch voltage clamp (p-p at 37°C), displayed spontaneous transient inward currents (STICs) at –74 mV, which were associated with a slowly developing outward current of varying amplitude (Ai, Bi) during depolarizing steps to positive potentials and a slowly decaying tail current upon repolarization to –54 and then –64 mV. In five typical SMCs voltage clamped with KCl-filled pipettes, membrane depolarization evoked a slowly developing current (I_{SS}) that was inward between –44 and –24 mV and outward at potentials more positive (Bi, Ci). This current and its associated slowly decaying tail current was still present after blockage of I_{KA} and BK channels with 2 mM 4-AP and 2 mM TEA (Bii, Cii), or after replacing the pipette K^+ concentration with Cs^+ (Di). (Cii, insert) When the mean relative amplitude of the tail currents (at –54 mV) in four cells was plotted against the preceding step potential and fitted with a sigmoidal Boltzmann equation, the resulting $V_{1/2}$ and *K* obtained were –12 and 7.4 mV, respectively. In CsCl-filled SMCs, the slowly developing inward and outward current and associated tail current was reduced by 1 μM nifedipne (Dii) and further blocked by the Cl^- channel blocker niflumic acid (100 μM NFA) (Diii), suggesting that this current is likely to be a Cl^- current that is activated in part by an influx of Ca^{2+} through L-type Ca^{2+} channels. Dashed line represents zero current; calibration bars apply to panels indicated.

and Ci). This current was distinguished by the slow time course of decay (deactivation) of its tail current when the membrane returned from positive potentials to –54 mV (for 100 ms) and then to –64 mV (Figure 3Bi). When the mean relative amplitude of these tail currents at –54 mV ($n = 4$) was plotted against the membrane potential during the preceding test potential, the resulting activation curve was maximal near 0 mV. The sigmoid Boltzmann equation fitted to the rising phase of this activation curve had a $V_{1/2}$ of –12 mV and a *K* of 7.4 mV (insert, Figure 3Cii). The cell properties of these typical SMCs with a slow tail current (capacitance 20.03 ± 2.96 pF, 2.42 ± 0.68 GΩ; $P > 0.05$ $n = 13$) were not significantly difference from typical SMCs without a tail current recorded with Kgluconate : KCl-filled pipettes (Table 1).

The application of TEA (2 mM) and 4-AP (2 mM) to four typical SMCs with a tail current, while blocking I_{KA} (Figure 3Bii and Cii, hollow circles) and BK channel activity, had little effect on the slowly developing outward current and its associated inward tail current (Figure 3Bii and Cii). In three cells recorded with CsCl-filled pipettes to block all current flow through K^+ channels, a component of the inward and outward current recorded upon membrane depolarization and the tail current upon membrane repolarization was reduced by nifedipine (1 μM) and blocked by 100 μM niflu-

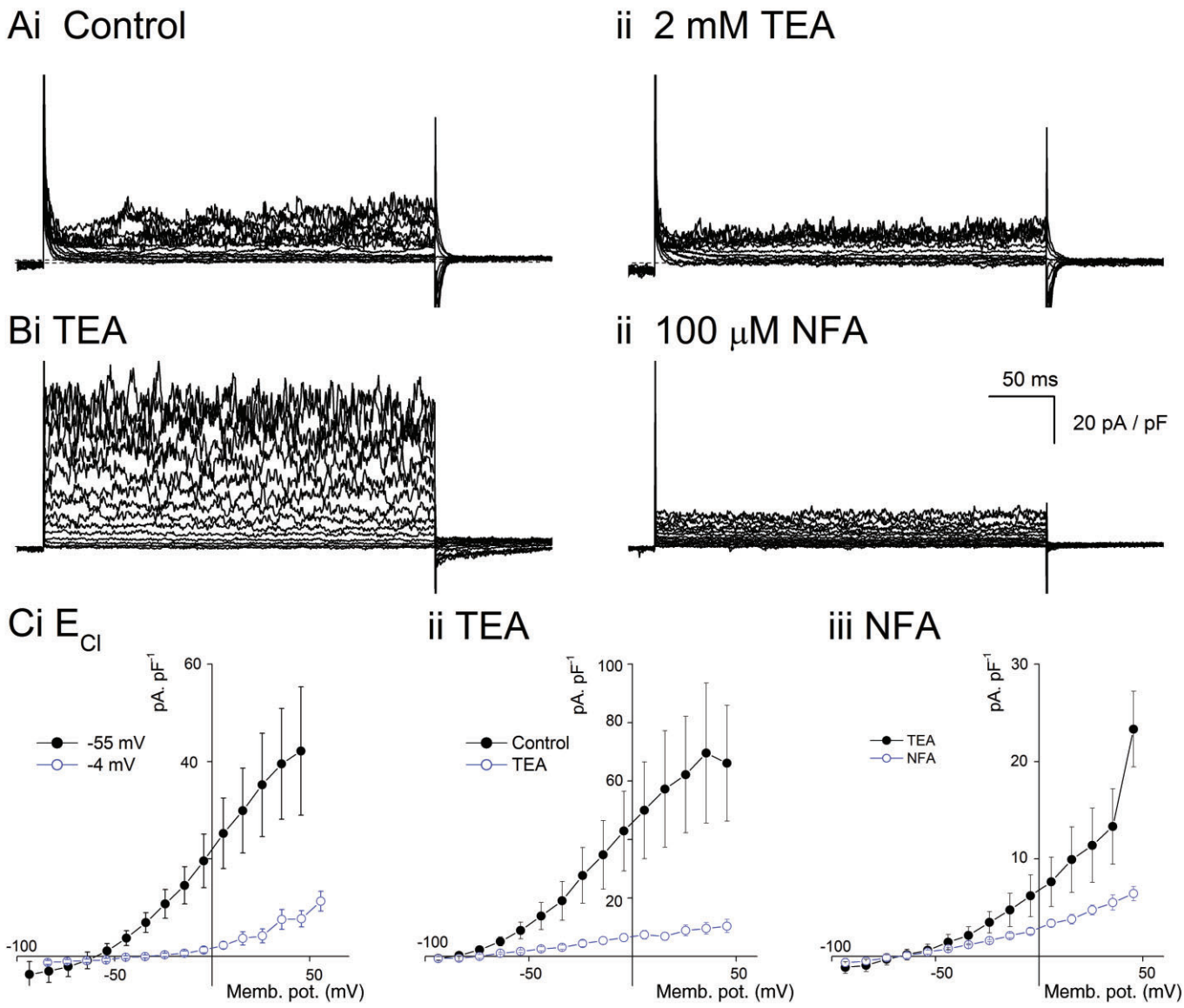

Figure 4

Electrical properties of atypical SMCs. Atypical cells were distinguished by the absence of I_{KA} and BK channel STOCs upon membrane depolarization. Membrane currents in cells voltage clamped with pipettes containing either KCl (130 mM) (Ai) or a Kgluconate (115 mM) : KCl (15 mM) mixture (Bi) were evoked by step depolarizations to potentials every 10 mV between –74 and 56 mV. Dashed lines represent zero current; calibration bar applied to all panels. (Ci) The steady-state current (I_{SS}) recorded over the last 5 ms of each depolarizing step was normalized for cell capacitance, averaged and plotted against membrane potential in 12 cells filled with the Kgluconate : KCl mixture and five KCl-filled cells for comparison. (Cii) I_{SS} normalized and averaged from six atypical SMCs voltage clamped with Kgluconate : KCl-filled pipettes were reduced at all potentials after 10 min exposure to 2 mM TEA. (Ciii) In the presence of TEA, I_{SS} in five cells was further reduced in the presence of the Cl^- channel blocker niflumic acid (NFA 100 μM).

mic acid (NFA; $N = 3$). These data suggest that typical SMCs also express Cl^--selective channels that may be Ca^{2+}-activated (Leblanc *et al.*, 2005).

Properties of atypical SMCs

The second population of eYFP-α-SMA^+ SMCs ($n = 8$, $N = 4$) recorded with the nystatin perforated-patch voltage clamp technique (at 37°C) displayed only a small increase in I_{SS} with membrane depolarization, which was associated with an increased current noise at positive potentials (Figures 1D and 4). In similar KCl-filled atypical SMCs ($n = 8$ $N = 6$) obtained from conventional mice, these noisy currents recorded at positive potentials were reduced by TEA (2–3 mM) (Figure 4Ai–ii and Cii), or 30 nM iberiotoxin ($n = 2$), suggesting that these current fluctuations arose from the opening of a few BK channels. It should be noted that these atypical SMCs never displayed large TEA-sensitive STOCs as displayed by typical SMCs (Figure 2Aiii).

Table 1
Properties of isolated single cells of the mouse renal pelvis

	Typical SMCs	Atypical SMCs	ICs
Cell length (μm)	64.2 ± 6.2	21.3 ± 2.6*	34.6 ± 4.0*
N	11	12	20
Capacitance (pF)	20.04 ± 1.12	12.96 ± 1.92*	16.97 ± 1.96
Membrane Resistance (GΩ)	2.74 ± 0.52	6.45 ± 2.08*	5.4 ± 1.58
N	37	10	9

Mean ± SEM.
*$P < 0.05$.

When the Nernst potential for Cl^- (E_{Cl}) in atypical SMCs was shifted from –4 to –55 mV using pipette solutions containing 115 mM Kgluconate : 15 mM KCl (n = 12 N = 12) (Figure 4Bi) instead of KCl (130 mM n = 5 N = 5) (Figure 4A), I_{SS} and its superimposed noisy fluctuations were larger at all potentials. In 15 of 44 cells, this larger outward current in Kgluconate was associated with a small slowly decaying tail current upon repolarization to –64 mV (Figure 4Bi). The mean *I–V* plot of 12 cells recorded with Kgluconate : KCl-containing pipettes (Figure 4Ci) displayed a greater slope conductance at 0 mV than KCl-filled cells (n = 5; Figure 4Ci). In five Kgluconate : KCl-filled atypical SMCs bathed in 2 mM TEA, I_{SS} and the following tail current were reduced by NFA (100 μM) (Figure 4B and Ciii). These data suggest that atypical SMCs also express Cl^--selective channels, which exhibit a marked outward (upward) rectification at potentials positive to E_{Cl} (Britton *et al.*, 2002; Leblanc *et al.*, 2005).

Table 1 summarizes the basic morphological and electrical properties of typical and atypical SMCs dispersed from conventional mice, as calculated from the time course of the capacitance artefacts evoked during small (5 mV) hyperpolarizing steps. It can be seen that the significantly larger cell lengths of typical SMCs compared with atypical SMCs was consistent with the significant difference in their membrane capacitances. The significantly larger input resistance of atypical SMCs is also consistent with the relatively few BK and Cl^--selective channels opened upon membrane depolarization.

We have interpreted the data above to conclude that I_{KA}-containing SMCs are typical SMCs, as these cells display many of the electrical properties of typical SMCs dispersed from the mouse ureteropelvic junction (Lang *et al.*, 2007c) or rat and guinea-pig ureter (Lang, 1989; Smith *et al.*, 2002) recorded using standard whole-cell voltage clamp techniques (at 22°C). We suggest that SMCs lacking I_{KA} are atypical SMCs.

Spontaneous currents in atypical SMCs

Atypical SMCs (30 cells of 54 examined), which were perforated-patch voltage clamped using Kgluconate : KCl-containing pipettes, held at –74 mV and bathed in 2–3 mM TEA and 1–3 μM nifedipine (at 35°C), were not electrically quiescent but displayed spontaneous inward currents. Atypical SMCs displayed STICs (<10 pA at –74 mV) that could be attributed to the opening of channels of differing ionic selectivity; both Cl^--selective channels and cation-selective channels. In fact, bursts of both cationic and Cl^--selective STICs could be recorded simultaneously in some cells. Figure 5A is representative of one of these cells, illustrating that current flow through all STICs was inward at –75 and –55 (near E_{Cl}) mV. However, at –35 mV, both inward and outward STICs were recorded, while all STICs were outward at –25 mV or potentials more positive (Figure 5A). We have interpreted these data as reflecting the presence of Cl^--selective STICs, which reversed near –55 mV and were outward at –35 mV, as well as cationic-selective STICs, which reversed between –35 and –25 mV.

Both cationic and Cl^--selective STICs appeared to sum to form large inward currents (LICs) (Figure 5Bi and Ci) that were 10–100 s of pA in amplitude, 10 to 100 s of ms in duration and which could also be separated by long periods of quiescence, compared to the high-frequency, small-amplitude STICs recorded at the same potential in the same cell (Figure 6A, B and Ci).

The reversal potential of the ion channels opened during bursts of STICs or individual LICs was established by comparing the membrane currents recorded by a ramp depolarization applied in the absence and presence of these spontaneous events (Figures 5Bii, Cii and 6Aii–iii). Ramp depolarizations (500 ms duration) applied during bursts of short-duration STICs revealed that these transients were inward of the ramp current at potentials negative of –50 mV and outward at potentials more positive. In nine atypical SMCs, that were perforated-patch voltage clamped using Kgluconate : KCl-containing pipettes, the reversal potential of the ramp current recorded during longer-lasting LICs was negative of –50 mV, near E_{Cl} (Figure 5Ci–ii). The Cl^- selectivity of these STICs and LICs was confirmed as they were readily blocked by 100 μM NFA (n = 4).

In nine other atypical SMCs, their STICs and LICs were observed to reverse at potentials more positive. In fact, the mean reversal potential of these LIC currents was –24.9 ± 5.3 mV (n = 5) when 115 Kgluconate : KCl-filled pipettes were used and –10.8 ± 5.1 mV (n = 4) when KCl-filled pipettes were used ($P < 0.05$) (Figure 6Aiii), suggesting a cationic selectivity of the channels opened during these spontaneous events. These cation-selective STICs were also reduced in amplitude upon reducing the extracellular Na^+ concentration to 30 mM (replaced with TEA). This reduction was associated

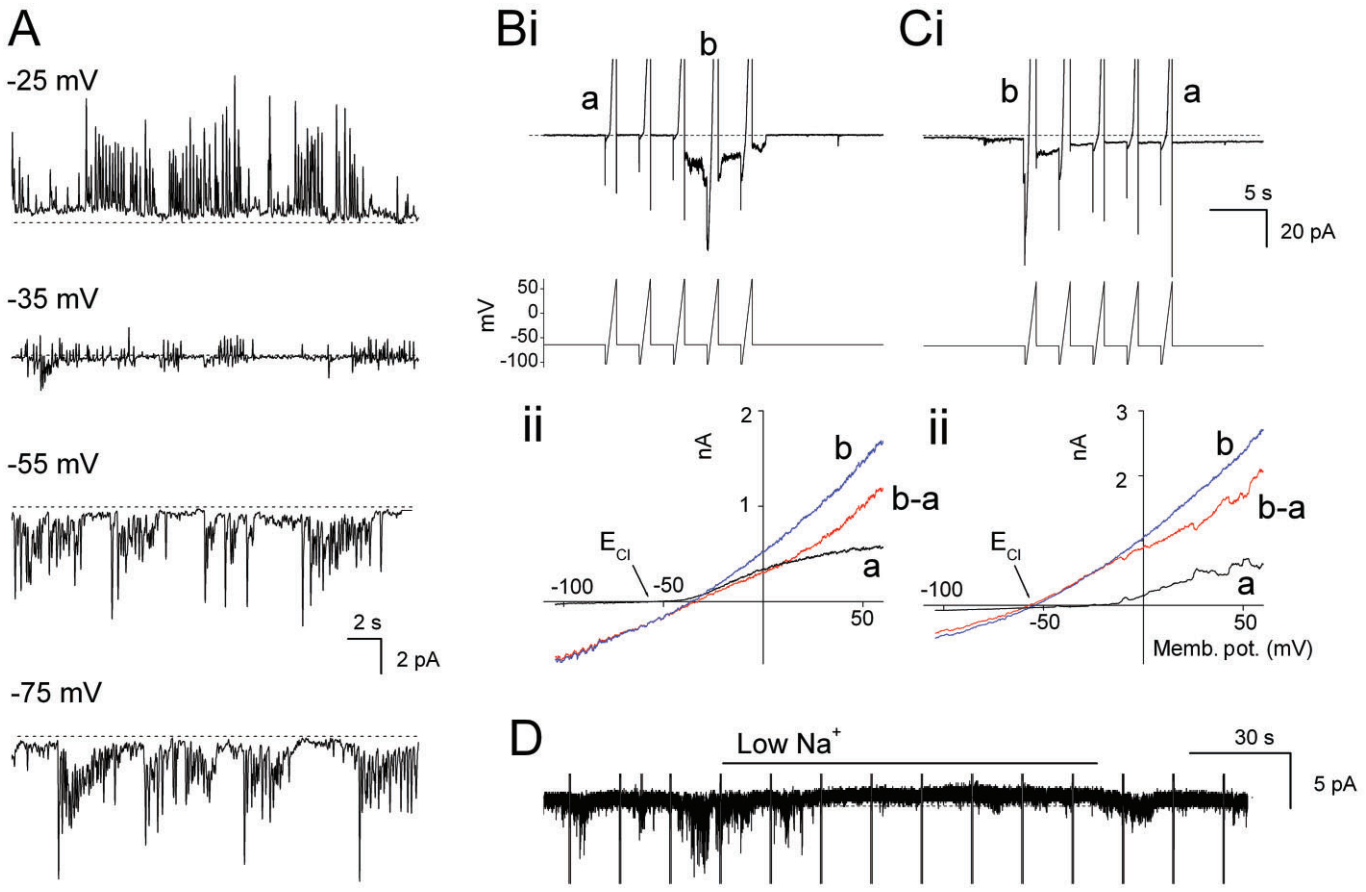

Figure 5

Spontaneous inward currents in atypical SMCs. (A) Illustrates bursts of STICs in a single atypical SMC at various holding potentials recorded under nystatin perforated patch voltage clamp (at 37°C) with Kgluconate : KCl-filled pipettes. Dashed lines represent zero current. Reversal potentials of spontaneous inward currents were either near −30 mV (b-a red line, Bii) or negative of −50 mV (b-a red line, Cii) as obtained upon subtraction of the membrane current evoked in response to a ramped depolarization during a spontaneous event (b blue line, Bii, Cii) from the ramp current evoked in their absence (a black line, Bii, Cii), E_{Cl} is set at −55 mV. (D) Replacement of external Na^+ (115 mM) with an equimolar concentration of TEA reduced the holding current and STIC activity.

with a decrease in the holding current of 2.8 ± 0.89 pA (n = 7 significantly different from 0 $P < 0.05$) and a reduction in the root mean square (RMS sampled over 10 s) of the holding current from 0.60 ± 0.22 to 0.31 ± 0.07 (n = 11, $P < 0.05$) (Figure 5D). In contrast, 3–10 mM TEA added to the bath had little affect on the holding current or its RMS (data not shown).

The notion that LICs discharge represented the flow of current through open channels, rather than a temporary loss or degradation of the integrity of the voltage clamp was confirmed in five cells by the use of the non-selective blocker of some transient receptor potential (TRP) channels, $LaCl_3$ (100 μM) (Alexander *et al.*, 2011), which rapidly blocked LIC discharge recorded at −74 mV in a manner that was partially reversed upon wash out (Figure 6B and C).

Electrical properties of α-SMA⁻ ICs

We have previously demonstrated that ICs (Figure 7A) freshly isolated from the distal renal pelvis recorded with the whole-cell voltage clamp technique and KCl-filled electrodes (at 22°C) were distinguished by the presence of a slowly activating and inactivating outward current (I_K) that was evident at potentials positive to −30 mV in the presence of TEA (2–3 mM) and 4-AP (2 mM) (n = 6, N = 6; Figure 7Bi–ii) (Lang *et al.*, 2007c). However, when ICs (n = 27, N = 15) were voltage clamped using Kgluconate : KCl-containing pipettes and nystatin perforated patches (at 37°C), this K^+ current often displayed more rapid kinetics of activation and inactivation, as well as large STOCs that were partially blocked by 2 mM TEA (Figure 7Bi–ii). In five ICs, the I_K remaining in the presence of TEA (2 mM), 4-AP (2 mM) and nifedipine (3 μM) was blocked in a concentration-dependent manner by 1–10 μM Xe991, a blocker of K_V7 channels (Figure 7C) (Mackie and Byron, 2008). Interestingly, the K_V7 channel activator, meclofenamic acid (MCA 20 μM) did not increase I_K (Anderson *et al.*, 2009). In fact, MCA (20 μM) partially reduced I_K. In addition, MCA did not prevent the inhibitory action of Xe991 (10 μM n = 4) (Figure 7Di–ii).

When ICs were examined with pipettes containing Kgluconate : KCl and nystatin perforated patches (at 37°C), small-

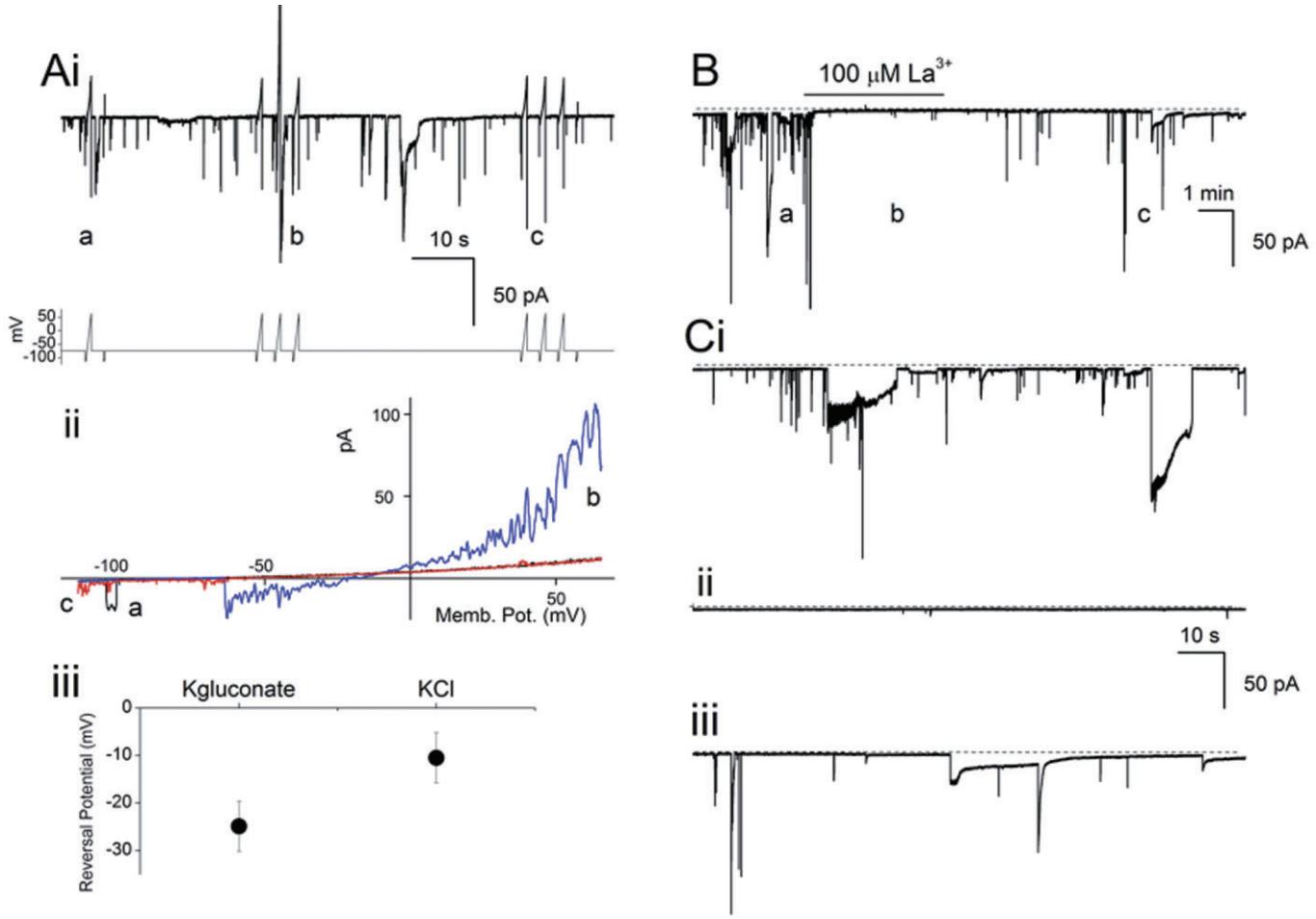

Figure 6

Properties of cationic LICs in the mouse renal pelvis. (A) The reversal potential of cationic LICs was obtained upon superimposition of the membrane current evoked in response to a ramped depolarization during a spontaneous event (Ai–iib) onto a control ramp current (Ai–iia). (Aiii) Plot of LIC reversal potentials when KCl (130 mM)- or Kgluconate (115 mM) : KCl (15 mM)-filled pipettes were used. (B) LIC discharge was reversibly blocked by the non-specific TRP channel blocker La^{3+}. (Ci–iii) Sections of (B) indicated by a-c have been displayed on an expanded time scale for better comparison. Calibration bar applies to all panels.

amplitude STOCs and STICs were often recorded when the holding potential was –74 mV. During stepped (Figure 7Bi–ii), ramped or maintained (Figure 8Ai–iii) depolarization to potentials positive to –50 mV, STOCs were reduced but not blocked in the presence of 2–3 mM TEA (Figure 8Aii–iii; n = 15 cells) and little affected upon the further addition of Xe991 to block I_K (10 μM) (Figure 7Cii–iii).

Under this regime of multiple K^+ channel blockers (TEA, 4-AP and Xe991), it was clear that the current flow during a STIC (at –74 mV) reversed in direction at potentials near –50 mV (Figure 8D). As E_{Cl} was set at –55 mV, we believe that the short duration STOCs recorded at positive potentials reflected current flow through Cl^--selective channels, and that these channel openings are responsible for the STICs recorded at –74 mV. This was confirmed as STICs at –74 mV and STOCs at potentials positive to –50 mV (Figure 8Bi–ii) were blocked by NFA (100 μM n = 4). Finally, all STOC and STIC discharge in the absence or presence of TEA and 4-AP was reduced by 30 μM ryanodine, the depletor of internal Ca^{2+} stores (n = 4; Figure 8Ci–ii).

Intracellular microelectrode recordings of typical SMCs

We have examined the functional role of the membrane currents identified in the single cell experiments above by investigating the effects of our selective blockers on the frequency and time course of the spontaneous action potentials recorded in the typical SMC layer in the intact preparation using standard intracellular microelectrode recording techniques. Impalements of the SMC wall with a single microelectrode invariably revealed the presence of spontaneous action potentials. In 10 of 40 impalements, action potential discharge initially consisted of two wave forms: a short-duration action potential (amplitude 37.9 ± 2.2 mV, $^1/_2$ width 519 ± 17.6 ms and frequency 7.5 ± 1.3 min^{-1}) (Figure 9Aiib and a lower frequency, longer action potential (amplitude

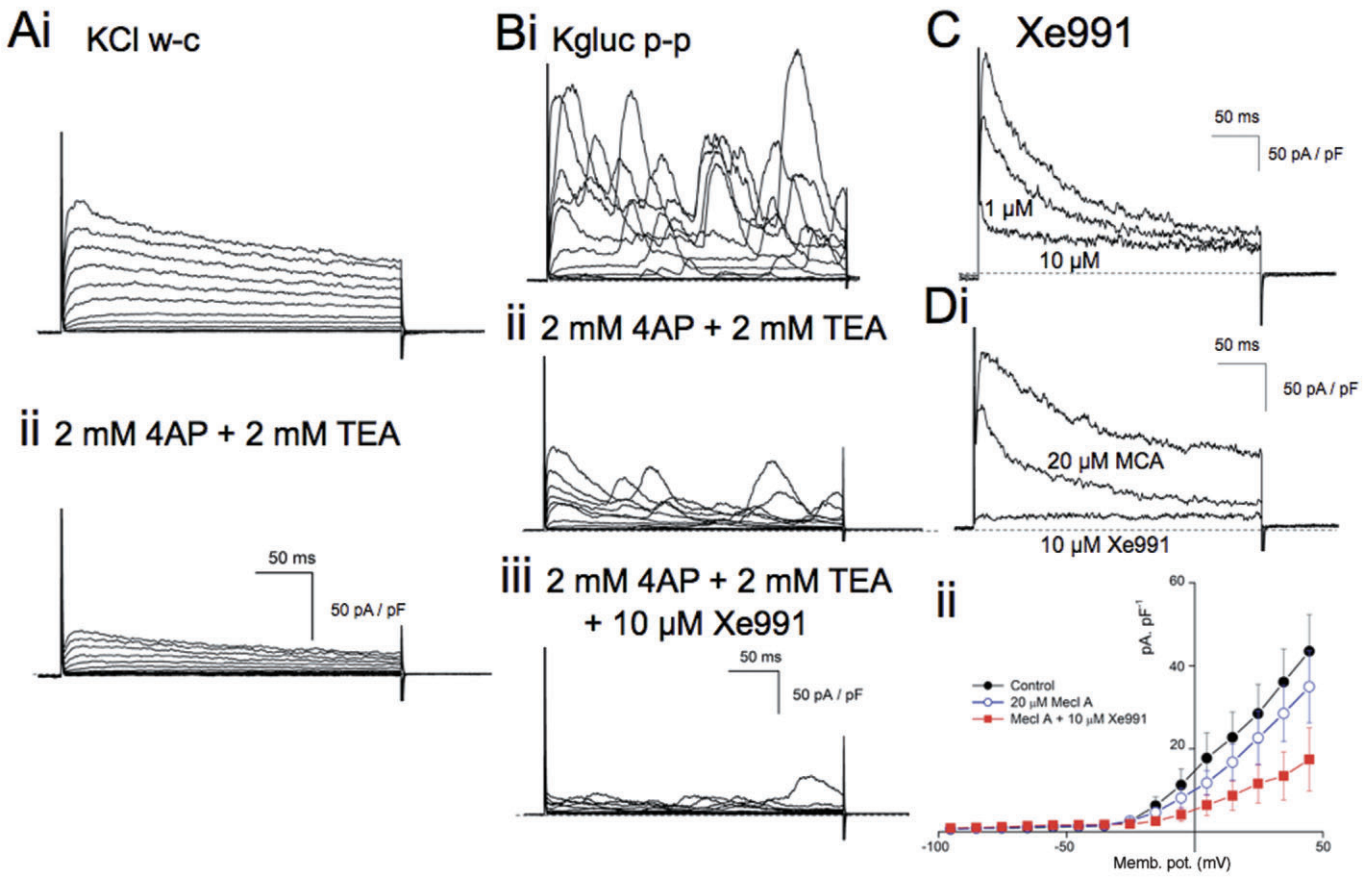

Figure 7

Electrical properties of ICs in the mouse renal pelvis. (Ai, Bi) Comparison of the time course of the outward currents recorded during depolarizing steps applied to ICs using KCl-filled pipettes and whole cell voltage clamp techniques (at 22°C) (Ai) or Kgluconate : KCl-filled pipettes and the perforated-patch voltage clamp (at 37°C) (Bi). Under both recording conditions, ICs were characterized by the presence of an I_K that was insensitive to TEA (2 mM) or 4-AP (2 mM, Aii, Bii). (Bii, C) This I_K was blocked in a concentration-dependent manner by Xe991 (1 and 10 μM), the selective blocker of K_V7 channels. However, this I_K was not increased but reduced by the K_V7 channel opener, meclofenamic acid (20 μM MCA, Di–ii). (Dii) Plot of I_{Peak} of I_K in four cells in control physiological saline, after to 10 min exposure to 20 μM MCA and another 10 min exposure to MCA plus 10 μM Xe991.

48.1 ± 2.6 mV, $^1/_2$ width 2281 ± 593 ms and frequency 2.4 ± 0.6 min^{-1}; n = 7 all $P < 0.05$) (Figure 9Aiia). With time (>5–10 min), these longer action potentials disappeared; the action potentials remaining increased in duration and fired at a regular frequency (Figure 9Ai). Thus, control action potentials were 41 ± 1.7 mV in amplitude, had a $^1/_2$ amplitude duration of 50.4 ± 41.1 ms, occurred at a frequency of 11.8 ± 1.0 min^{-1} and discharged from a resting membrane potential of –56.0 ± 2.0 mV (n = 30, N = 10) (Figure 9Aiic).

Pre-exposure of tissues to tetrodotoxin (0.1 μM for 5–10 min, n = 6) had no noticeable effects on the frequency or time course of the recorded action potentials (data not shown). The effects of applied agents in the absence or presence of TTX on action potential parameters were therefore pooled before presentation. Figure 9A–E illustrates the effects of TEA (2 mM), 4-AP (2 mM), NFA (100 μM) and Xe991 (Xe 10 μM) applied to the mouse renal pelvis, while Figure 9F summarizes their relative effects on the membrane potential, initial action potential amplitude, $^1/_2$ width and interval between action potentials. Percentage changes in action potential parameters were expressed as 100 × (C – T)/C, where C was the mean value measured during the 2 min period preceding the application of a channel blocker, while T represents the mean value measured over 2 min, 6–8 min after commencement of the drug exposure.

Both TEA and 4-AP significantly depolarized the membrane 7.4 ± 2 (n = 7) and 6.5 ± 1.5 mV (n = 6 both $P < 0.05$), respectively. In comparison with the sustained membrane depolarization evoked upon TEA exposure, the depolarization to 4-AP was transient, so that after 6–8 min, the membrane potential was only 2 ± 1.5 mV positive of control (n = 6, $P > 0.05$).

TEA significantly increased the action potential $^1/_2$ width by 195.5 ± 4.9% and decreased their interval between events by 20.3 ± 11.3% (n = 8 both $P < 0.05$) (Figure 9Bii, Cii and F). There was also a noticeably more distinct, albeit not significantly larger initial spike in the presence of TEA or 4-AP (Figure 9Bii and Cii). In comparison, NFA (100 μM) increased

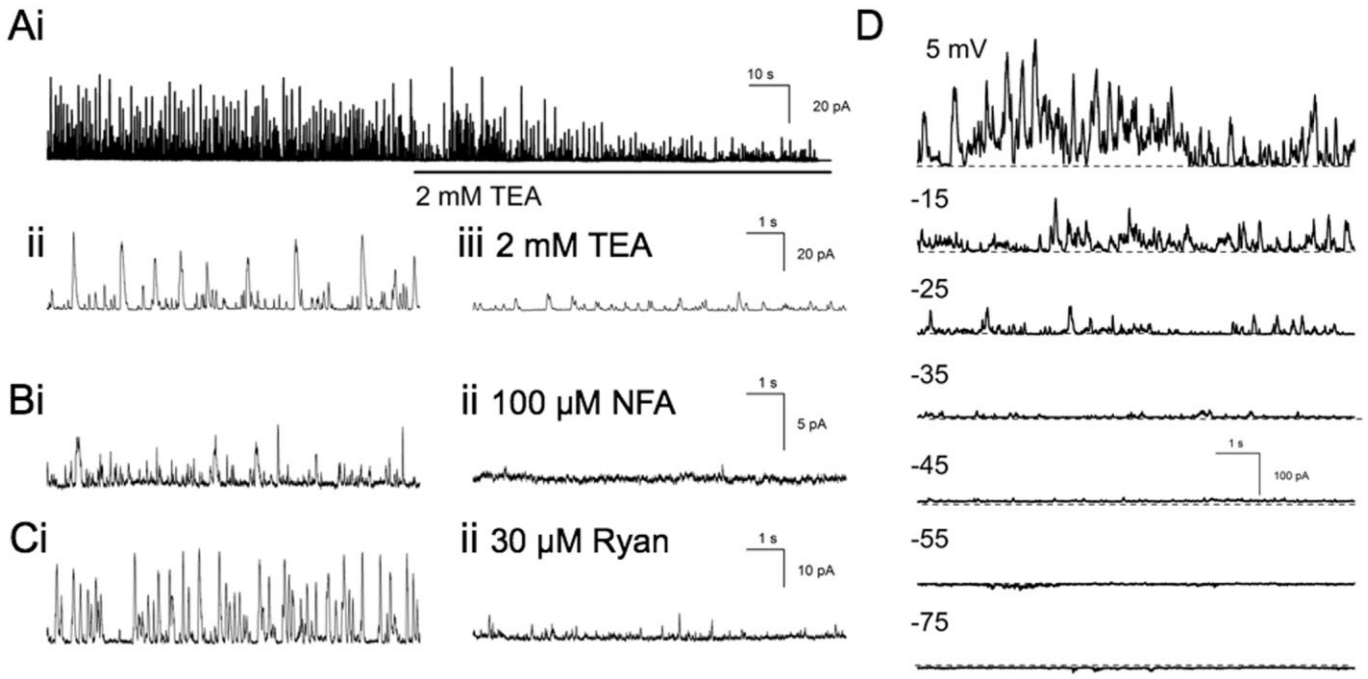

Figure 8

Spontaneous currents in ICs. (A) STOCs recorded at positive potentials (+4 mV Ai) in ICs (at 37°C) bathed in 1 μM nifedipine were only partially reduced in the presence of the BK channel blocker TEA (2 mM, Ai). (Aii–iii) Portions of (Ai) in the absence and presence of TEA on an expanded time base for better comparison. (Bi–ii) STOCs remaining in TEA were blocked by NFA (100 μM) or upon depletion of internal Ca^{2+} stores with ryanodine (30 μM, Ci–ii). (D) The STOCs remaining in TEA had a reversal potential near −50 V, suggesting that these spontaneous events represented the outward flow of current through Cl^--selective channels.

the interval between action potentials by 50.3 ± 8.2% (n = 4 P < 0.05) (Figure 9D and F), while 10 μM Xe991 decreased their interval by 31.1 ± 12.7% (n = 6, P < 0.05) (Figure 9E and F). The membrane potential and other action potential parameters were not significantly affected by NFA or Xe991 (P > 0.05) (Figure 9Dii, Eii and F).

Immunohistological studies of the renal pelvis

The data above suggest that typical and atypical SMCs and ICs are distinguishable electrophysiologically by their K^+ and Cl^- channel expression. We have therefore made a systematic examination for the presence of the likely subunits of the ion channels identified in coronal sections of the mouse renal pelvis using standard immunohistological techniques and fluorescence microscopy. We also examined the rat renal pelvis to establish whether a similar distribution was present in another mammalian species (Figure S2C). We have applied monoclonal or polyclonal antibodies raised against K_V4.3, ANO1/ TMEM16A and K_V7.5 channel subunits after double labelling with control antibodies against α-SMA, phosphorylated neurofilament PGP9.5 as well as the Kit antibody, AK2 (Metzger *et al.*, 2005). Photomicrographs of proximal and distal regions of the renal pelvis were taken under the same settings for contrast and illumination for better comparison. In almost all cases, the urothelium, parenchyma (Figure 11Cii, insert) and the adipocytes in the fat (Figure 10Biv) surrounding the kidney displayed some degree of fluorescence in the absence of our antibodies, particularly when polyclonal antibodies were used. However, these structures proved useful markers in terms of orientating the various regions of the renal pelvis.

Sections of kidneys obtained from eYFP-α-SMA^+ transgenic mice when fixed with 4% paraformaldehyde readily displayed the changing profile of α-SMA^+ cells with distance from the base of the papilla (N = 4; Figure S1B–D) observed previously in the guinea-pig (Klemm *et al.*, 1999) and rat (Lang *et al.*, 2001) using the electron microscope. Unfortunately, when fixed in acetone, sections from these mice rapidly leached upon illumination under fluorescent light. However, immunostaining of these sections with antibodies raised against α-SMA and a red secondary confirmed that the cells illuminated under blue light were in fact SMCs. The double immunostaining described below were therefore performed mostly on sections obtained from conventional mice, sections were also stained with the blue nuclear stain Hoescst 33342.

Double labelling of kidney sections fixed with acetone with anti K_V4.3 (N = 5; Figure 10A and B*) or anti-ANO1/ TMEM16A (N = 8; Figure 11) with anti-α-SMA revealed that both stains were located in the SMC layer, and that the immunoreactivity of all three antibodies was more intense in the distal regions of the renal pelvis compared with the base of the papilla (Figure 11A and C). In the distal regions of the rat renal pelvis, immunoreactivity of ANO1/ TMEM16A also co-located in the SMC layer (Figure S2Bi–ii).

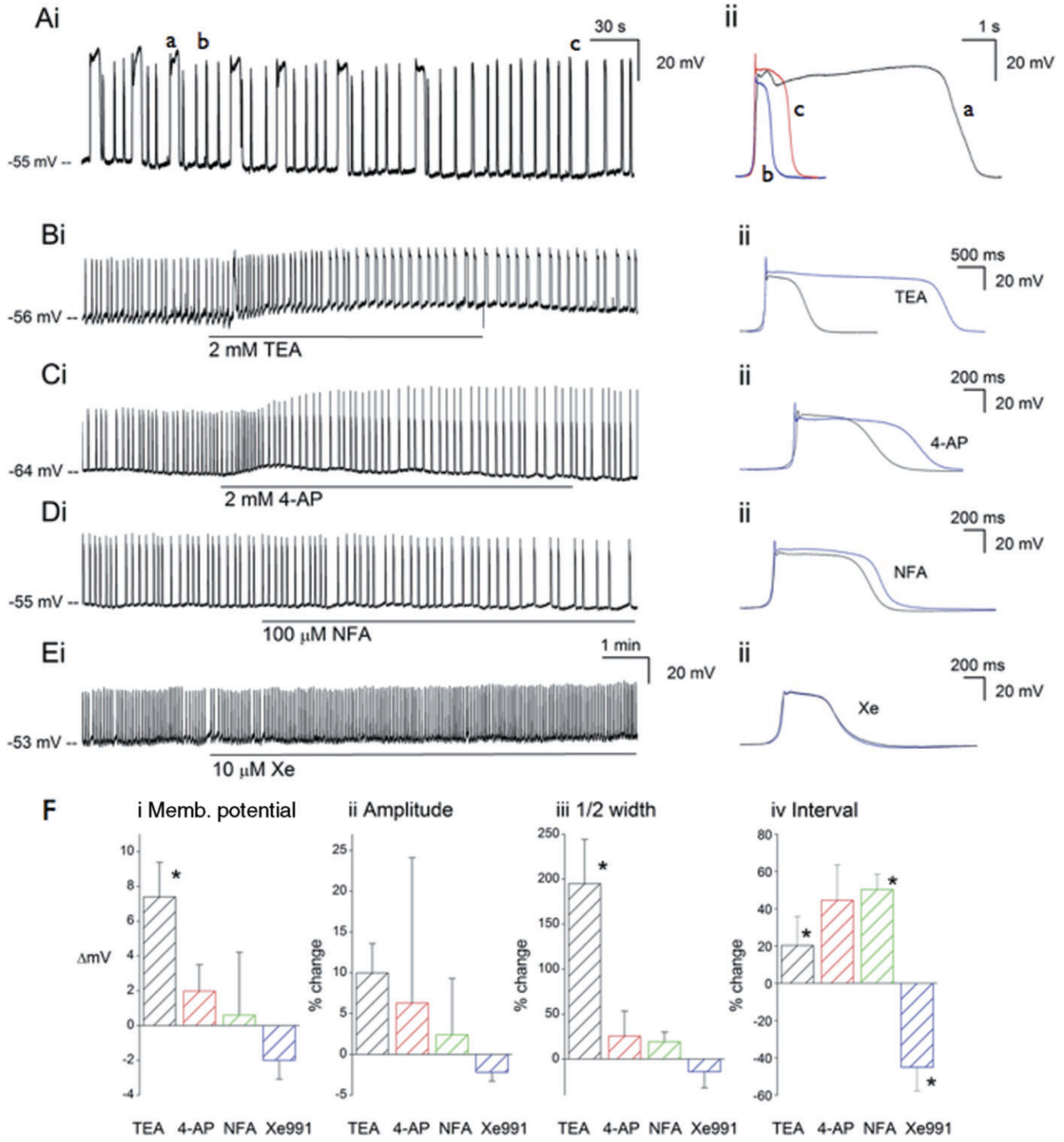

Figure 9

Effects of K^+ and Cl^- channel blockers on action potentials recorded in intact renal pelvis. (A) Example of intracellular microelectrode recordings of the typical SMC wall within the first 10 min of electrode impalement. Note that the infrequent long duration action potentials disappear with time. (Aii) Portions of the trace in (A) indicated by a-c are superimposed and plotted on an expanded time scale for a better comparison. Effects of blockers of K^+ channels, TEA (2 mM, Bi), 4-AP (2 mM, Ci) and Xe991 (XE 10 μM, Ei) and Cl^- channels, NFA (100 μM, Di) on the spontaneous action potentials recorded in the renal pelvis. (Bii, Cii, Dii, Eii) Five to eight action potentials in the absence or presence of each agent have been averaged, superimposed and displayed on an expanded time scale. (F) Pooled effects of the K^+ and Cl^- channel blockers on the membrane potential (Fi) and distinguishing characteristics (Fii–iv) of the spontaneous action potentials in the renal pelvis in the absence or presence of TTX (1 μM). Percentage changes in action potential parameters were expressed as $100 \times (C - T)/C$, where C represents the mean value measured in the absence of the channel blocker, while T represents the mean value measured after 6–8 min exposure to the drug. * represents a significant ($P < 0.05$) difference from zero.

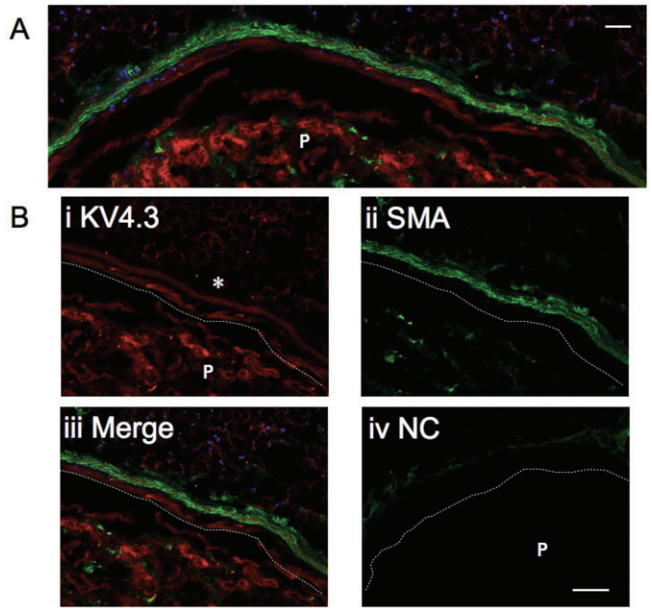

Figure 10

Distribution of α-SMA and $K_V4.3$ immunoreactivity in the mouse renal pelvis. Examples of photomicrographs of the distal region of the renal pelvis doubled labelled with the antibodies for $K_V4.3$ (A, red; Bi) and α-SMA (A, green; Bii). (Biii) Superimposed micrographs of $K_V4.3$ and α-SMA staining reveals that the smooth muscle layer (Bi*, ii) and cells within the suburothelium space stain for $K_V4.3$. This staining was more intense in the distal regions of the renal pelvis. (Biv) A negative control (NC); the dashed line in all panels represents the luminal surface of the urothelium, and P indicates the papilla. Calibration bar for all panels represents 50 μm.

Intense immunoreactivity for ANO1/ TMEM16A Cl^- channel subunits was also present in α–SMC^- ICs in the proximal and mid regions of the renal pelvis, located in the suburothelial region (Figure 11Ci) as well as in regions serosal to the layer of α–SMC^+ cells (Figure 11). These ANO1/ $TMEM16A^+$ α–SMC^- ICs were most evident in the proximal and mid regions of the renal pelvis.

In contrast, $K_V4.3$ and $K_V7.5$ immunoreactivity were both evident in α-SMA^- ICs located within the suburothelium region of the renal pelvis (Figure 12). These $K_V7.5^+$ cells were clearly stellate in appearance and densely distributed in the distal renal pelvis, forming a distinct suburothelial layer adjacent to the stratified transitional epithelium that make up the luminal surface of the urothelium. In the proximal regions of the renal pelvis near the base of the papilla, the transitional epithelium consists only of elongated $K_V7.5^+$ ICs (Figure 12C). Little or no $K_V7.5$ immunoreactivity was found in the α-SMA^+ muscle layer. $K_V7.5^+$ ICs (Figure 12) in the suburothelium and serosal ANO1/ $TMEM16A^+$ ICs both formed close associations with like-staining cells, perhaps forming interconnecting networks.

The preferential immunostaining of ICs in the present experiments to antibodies against ANO1/ TMEM16A, promoted a re-examination of Kit immunoreactivity of ICs in the mouse renal pelvis. Using well-established methods for staining of ICCs in the intestine (Figure S2Aiii) (Komuro, 1999), double labelling of coronal sections of mouse renal pelvis with antibodies for markers of the smooth muscle wall (anti-TMEM16A/ ANO1 or anti-α–SMA) with anti-Kit (AK2), or whole mounts (Figure S2Ai–ii) with anti-Kit (AK2) and anti-PGP9.5, indicated that Kit staining was not located in ICs or SMCs, but most likely located in the $PGP9.5^+$ nerve bundles (Zhang and Fedoroff, 1997).

We also used sections of mouse proximal colon as positive controls to readily demonstrate that ANO1/ TMEM16A and Kit immunoreactivity co-located in cells adjacent to the myenereric plexus, which was intensely immunoreactive to PGP9.5 (Figure S2Aiii) or $K_V4.3$ (data not shown), as well as to cells located on the serosal surface of the longitudinal muscle layer. Kit immunoreactivity was also observed in the cell bodies of the mouse and rat supra-optic nucleus but not in the optic chiasm, while ANO1/ TMEM16A immunoreactivity was located in the blood vessels in these brain regions (data not shown).

Discussion

In the intact renal pelvis, there is increasing evidence that STD discharge in atypical SMCs is likely to be responsible for triggering the regenerative action potentials, Ca^{2+} waves and propagating muscle contractions underlying pyeloureteric peristalsis. We envisage that synchronization of spontaneously-firing STDs into a pacemaker signal that triggers a propagating action potential in the typical SMC layer is driven by the atypical SMC bundle firing STDs at the highest frequency so that only one pacemaker region would be apparent at any one time (Lang, 2010; Lang *et al.*, 2010). This mechanism involves a dynamic interaction between Ca^{2+} entry through L-type Ca^{2+} channels opened upon membrane depolarization, uptake and release of Ca^{2+} from endoplasmic reticulum and mitochondrial stores (Hashitani *et al.*, 2009) and the entrainment of Ca^{2+} release from both inositol trisphosphate (IP_3)- and ryanodine-receptor coupled Ca^{2+} stores (Lang *et al.*, 2007a,b; 2010). However, it is not clear whether these voltage-dependent Ca^{2+} entry and internal store-dependent components of the coupled oscillator reside exclusively within atypical SMCs themselves, or are distributed in both atypical and typical SMCs. In the present experiments, we have enzymatically dispersed the mouse renal pelvis into its constituent cells to characterize and distinguish atypical SMCs from typical SMCs and other α-SMC^- cells (ICs) on the basis of their ion channel expression and kinetics, and used this differential expression as a means of unequivocally locating these cells within the intact renal pelvis.

Typical SMCs

Whole-cell current recordings (at room temperature) from single SMCs from the guinea-pig (Imaizumi *et al.*, 1989; Lang, 1989) and rat (Smith *et al.*, 2002) ureter and the mouse ueteropelvic junction (Lang *et al.*, 2007c), regions in which atypical SMCs are not present, display I_{KA} and BK channel-dependent STOCs similar to the currents recorded in our typical SMCs in the present experiments (perforated-patch voltage clamp and 37°C). This has been confirmed with the use of the eYFP-α-SMA transgenic mice, which established

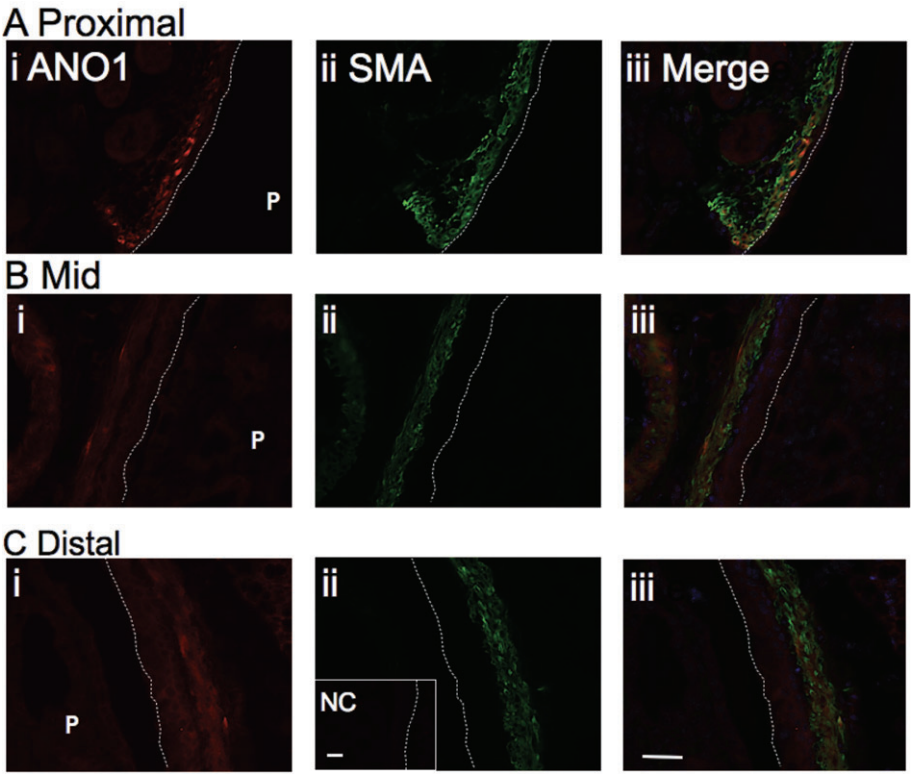

Figure 11

Distribution of ANO1/ TMEM16A and α-SMA immunoreactivity in the mouse renal pelvis. Examples of photomicrographs of the proximal (A), mid (B) and distal (C) regions of the same coronal section of the renal pelvis stained with the antibodies for ANO1/ TMEM16A (ANO1 red, Ai, Bi, Ci) and α-SMA (SMA green, Aii, Bii, Cii). (Aiii, Biii, Ciii) Superimposed micrographs of TMEM16A and α-SMA. TMEM16A staining was more intense in the distal regions of the renal pelvis and collocated with the more intense staining for α-SMA in the smooth muscle layer. TMEM16A immunostaining was also present in α-SMA$^-$ ICs in the suburothelial zone of the transitional epithelium (urothelium) and in the serosal regions of the proximal (Ciii) and middle (Mid, Biii) renal pelvis. The dashed line in all panels represents the luminal surface of the urothelium. (Cii, insert) A negative control; P represents the papilla. Calibration bar represents 50 μm for all panels.

that these I_{KA}-containing cells were of smooth muscle origin. Our immunohistological studies have also established that K_V4^+ α-SMA$^+$ SMCs were present in greater numbers and were packed more closely in the more distal regions of the renal pelvis where electron microscopy confirms that the muscle wall is made up of mostly typical SMCs (Gosling and Dixon, 1974; Klemm *et al.*, 1999) (Figure 13), and our microelectrode studies established that 'driven' action potentials were recorded in the majority of impalements (Figure 9) (Klemm *et al.*, 1999; Lang *et al.*, 2001).

The 'window current' generated by the overlapping activation and inactivation curves of I_{KA} suggests that these channels should contribute to the resting membrane potential, and this was confirmed in the intact tissue by the transient membrane depolarization observed in the presence of 4-AP (Figure 9Fi). BK channel openings also contribute to the membrane potential evident by the significant sustained membrane depolarization in TEA (Figure 9Fi). Both I_{KA} and BK channel openings would also be expected to oppose the depolarizing influence of Ca^{2+} entering through voltage-operated Ca^{2+} channels opened during the action potential and this is supported by the, albeit not significant, increase in amplitude (Figure 9Fii) and maximum rate of rise (data not shown) of the initial spike recorded in the presence of 4-AP or TEA. However, BK channel activation appears to be crucial to determining the action potential duration (Figure 9Cii) (Lang, 1989).

In common with SMCs isolated from the rat, but not guinea-pig ureter (Smith *et al.*, 2002) typical SMCs voltage clamped with KCl-filled pipettes often also displayed a slowly developing current upon membrane depolarization, associated with a slowly deactivating tail current upon repolarization, which was dependent on Ca^{2+} entry and reduced by NFA (Figure 3). Expression of many of the candidate proteins (CLCA, CIC-3, bestrophins and Tweety) for Ca^{2+}-activated Cl^- channels (CaCCs) into cell lines creates channels that do not mimic particularly well native CaCCs (Galietta, 2009). However, recent bioinformatic analysis and function genomic approaches have suggested that ANO1/ TMEM16A is a protein likely to form, or be intimately associated with CaCCs involved in secretion (Caputo *et al.*, 2008; Yang *et al.*, 2008; Galietta, 2009). Moreover, both *Xenopus* ANO1/ TMEM16A protein expressed in *Axolotl* oocytes (Schroeder *et al.*, 2008) and mouse ANO1/ TMEM16A protein expressed in HEK293 cells (Yang *et al.*, 2008) form CaCCs that display a slowly developing current

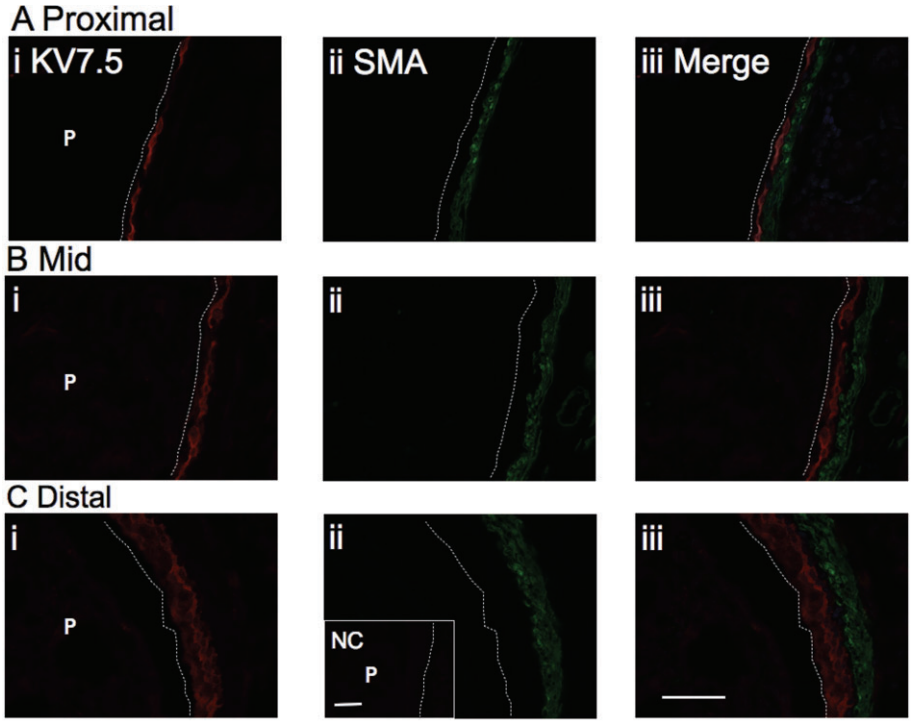

Figure 12

Distribution of KV7.5 channel subunit and α-SMA immunoreactivity in the mouse renal pelvis. Examples of photomicrographs of the proximal (A), mid (B) and distal (C) regions of the same coronal section of the renal pelvis double labelled with the antibodies against K_V7.5 (red, Ai, Bi, Ci) and α-SMA (SMA green, Aii, Bii, Cii). (Aiii, Biii, Ciii) Superimposed micrographs of K_V7.5 and α-SMA immunoreactivity. K_V7.5 staining was mostly restricted to a layer of densely packed ICs within the suburothelial region, particularly in the distal regions of the renal pelvis and occasionally observed in the serosa. These $K_V7.5^+$ ICs formed a single layer of elongated cells in the proximal (Ai) and mid (Bi) renal pelvis. The dashed line in all panels represents the luminal surface of the urothelium. (Ciii, insert) A negative control; P represents the papilla. Calibration bar represents 50 μm for all panels.

that is blocked by NFA, strongly outwardly rectifying when the internal Ca^{2+} concentrations are low (<1 μM) but displays a nearly linear *I–V* relationship when the internal Ca^{2+} is raised.

The likely presence of ANO1/ TMEM16A Cl^- channels in typical SMCs of the renal pelvis was confirmed by the higher density of this immunoreactive product in the distal regions compared with the proximal regions of the renal pelvis, in cells that were also more intensely immunoreactive for K_V4.3 and α-SMA (Figures 10 and 13; Figure S2B). This continues the region specific nature of smooth muscle expression of ANO1/ TMEM16A staining in the mouse, as it is found in airways smooth muscle, the oviduct and ductus epididymus, but not in the urethra or gastrointestinal tract (Huang *et al.*, 2009).

Atypical SMCs

A portion of the eYFP-α-SMA^+ cells did not display any voltage-operated K^+ currents, justifying the original designation by Gosling and Dixon as 'atypical' SMCs (Gosling and Dixon, 1972; Dixon and Gosling, 1973). The significantly smaller membrane capacitance of atypical SMCs, compared with typical SMCs (Table 1), is consistent with the relatively thin atypical SMCs observed under the electron microscope (data not shown).

The membrane channel complement, particularly the lack of any voltage-operated K^+ currents, of atypical SMCs appears to be unique in smooth muscle physiology. The increase in I_{SS} and current noise recorded during depolarizing steps to potentials negative of E_{Cl} applied during the initial phases of an experiment was best explained by the opening of relatively few BK channels. At potentials positive to E_{Cl}, the current noise during these depolarizing steps increased due to outward current flow through outwardly rectifying Cl^--selective channels that were sensitive to NFA blockade (Figure 4). At −74 mV, the opening of these channels was evident by the presence of small Cl^--dependent STICs also blocked by NFA (data not shown). Such a marked outward rectification makes it unlikely that these Cl^- channels make any sizable contribution to the large pacemaker currents readily recorded in these atypical SMCs (see below). It seems more likely these Cl^- channels, in conjunction with the activation of cation-selective STICs and BK channels (Figures 5 and 6), are involved in setting the membrane potential of these cells, as recently demonstrated in human and monkey colonic SMCs (Dwyer *et al.*, 2011).

The most striking property of atypical SMCs, bathed in the presence of the L-type Ca^{2+} channel blocker, nifedipine, was the ability of their STICs to amalgamate to generate LICs. Some of these LICs were Cl^--selective with reversal potentials

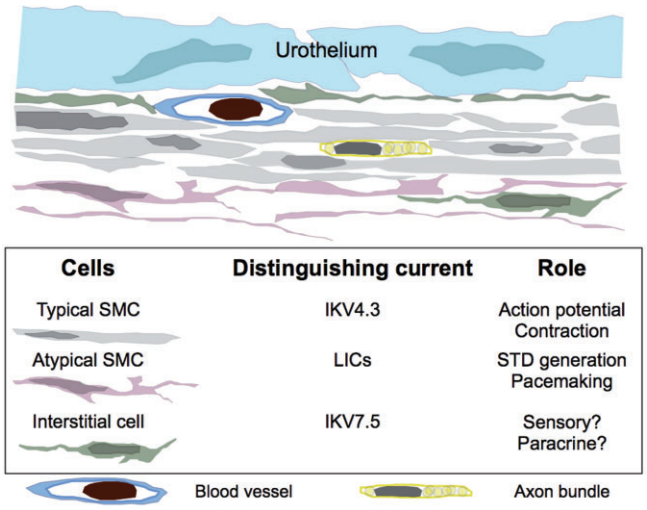

Figure 13

Summary of the arrangement and putative roles of the three cell types in the mouse renal pelvis identified electrophysiologically. Adjacent to the urothelium, KV4.3$^+$ ANO1/ TMEM16A$^+$ typical SMCs form a continuous muscle layer that gradually thickens from one to two cells thick at the papilla–pelvis border to four to six cells thick at the ureteropelvic junction to generate the contractions underlying pyeloureteric peristalsis. In contrast, atypical SMCs form distinct clusters of thin cells serosal to the typical SMC layer only in the proximal regions of the renal pelvis. KV7.5$^+$ KV4.3$^+$ ICs are present in greater numbers in the suburothelial space in the more distal regions of the renal pelvis, as well as being sparsely distributed in the serosa.

near E_{Cl}, while others had more positive reversal potentials which shifted only 14 mV when the E_{Cl} was shifted some 50 mV (Figure 6). Replacement of the external Na^+ with TEA or application of La^{3+} reduced STIC amplitudes and blocked LIC discharge. Similar demonstrations of inward currents with reversal potentials well positive of E_{Cl}, and sensitive to blockade by trivalent cations, has been reported in SMCs of human and monkey colon (Dwyer *et al.*, 2011), mouse urinary bladder (Thorneloe and Nelson, 2004) and rabbit ear artery (Albert *et al.*, 2006).

If LIC discharge does in fact underlie STD generation, a preferential selectivity for cations can perhaps be inferred from our previous observations that STDs recorded in the intact renal pelvis with intracellular microelectrodes are substantially reduced when the external Na^+ concentration is mostly (82%) replaced with N-methyl-D-glucamine, but little affected when 93% of the external Cl^- is replaced by isethionate. These STDs were also little affected by the Cl^- channel blocker 4,4′-diisothiocyanostilbene-2,2′-disulphonic acid (DIDS) (Lang *et al.*, 2007b). In the present experiments, the interval between action potentials, presumably driven by atypical SMC pacemakers, was increased approximately 50% by niflumic acid (Figure 9Fiv). Whether this reflects a change in the atypical SMC membrane potential or their LIC firing has yet to be established. Finally, irrespective of their ionic selectivity we propose that spontaneous LICs recorded only in atypical SMCs underlie the generation of the spontaneous STDs recorded in the intact tissue.

ANO1/ TMEM16A$^+$ and K_V7.5$^+$ ICs

When viewed with electron microscopy, ICs in the renal pelvis of guinea-pig (Klemm *et al.*, 1999) and rat (Lang *et al.*, 2001), fulfil many of the ultrastructural criteria for ICs of Cajal (ICC), the pacemaker cells of the gastrointestinal tract which are also distinguished by their immunoreactivity to Kit (CD117) (Komuro, 1999) and ANO1/ TMEM16A) (Gomez-Pinilla *et al.*, 2009; Zhu *et al.*, 2009). Spindle- or stellate-shaped Kit$^+$ cells have been reported to be sparsely distributed within sections of the urothelial layer, the lamina propria and the muscle layer in sections of the renal pelvis and proximal ureter in a number of mammals (Pezzone *et al.*, 2003; Metzger *et al.*, 2004; 2005; 2008; van der Aa *et al.*, 2004; David *et al.*, 2005). However, Kit (CD117) performs a number of essential roles in the development of the immune system and the physiology of various cells and is, therefore, also used to identify many other cells including bone marrow haematopoietic progenitors, melanocytes and mast cells (Hashitani and Lang, 2010).

In the present experiments, Kit immunoreactivity in sections or whole mounts preparations of fixed renal pelvis was located primarily in the nerves bundles (Figure S2Ai–ii), as has been demonstrated in nerve fibres and glial cells of the mouse brain (Zhang and Fedoroff, 1997). This may well be in agreement with both our failure to demonstrate in the mouse renal pelvis that Kit$^+$ FITC dextran $^-$ ICs (therefore unlikely to be macrophages) (Lang *et al.*, 2007a,b) fire the nifedipine-insensitive Ca^{2+} signals of low frequency and long duration that we have previously suggested to arise from 'ICC-like' ICs (Lang *et al.*, 2010) and the presence in the guinea-pig pyeloureteric system of a network of ICC-like ICs that are clearly Kit negative (Klemm *et al.*, 1999). Kit staining of nerve bundles in the renal pelvis would reconcile the loss of both nerve (Murakumo *et al.*, 1997; Solari *et al.*, 2003) and Kit immunoreactivity (Solari *et al.*, 2003; E Arena *et al.*, 2007; F Arena *et al.*, 2007; S Arena *et al.*, 2007; Kang *et al.*, 2009) observed in sectioned material during congenital ureteropelvic and ureteric obstruction. Thus, the present observations that ICs in the mouse renal pelvis are intensely immunoreactive to ANO1/ TMEM16A and K_V7.5 antibodies suggest that channel profiling via immunohistochemistry may prove to be a more selective means than Kit of identifying 'ICC-like' ICs in the upper urinary tract.

It is not yet clear whether all ANO1/ TMEM16A$^+$ ICs are also K_V7.5$^+$, and *vice versa*, although the electrophysiological evidence suggests they may well be. We have demonstrated that immunoreactive products for both antibodies were located in the suburothelial zone, and that these cells were more densely distributed in the distal renal pelvis (Figures 11–13). However, we only occasionally saw immunoreactive product for K_V7.5 in ICs located within the serosa where the presence of ANO1/ TMEM16A$^+$ ICs was commonly observed. Single ICs of the guinea-pig bladder also display a Xe991-sensitive K^+ current (Anderson *et al.*, 2009), although it is not clear whether these cells were Kit or vimentin positive, or immunoreactive to both antigens. In our hands, Kit and ANO1/ TMEM16A immunoreactivity was best observed after acetone fixation, while the K_V7.5$^+$ ICs were only observed in kidneys undergoing our 2% paraformaldehyde followed by acetone fixation. If the presence or absence of

this co-location is better established under other fixing and processing regimes, then the examination of pelviureteric tissues for ICs containing combinations of Kit, vimentin, ANO1/ TMEM16A and K_V7.5 immunoproducts may well reveal a highly developed region-specific distribution of ICs in the renal pelvis as has been established in the bladder. The examination of this regional distribution under normal and various pathological conditions, occurring congenitally or induced experimentally, may well provide considerable insights into the function of these cells and their reprogramming with hydronephrosis.

In summary, this report represents the first electrophysiological distinction between typical and atypical SMCs in the mouse renal pelvis, while their differing ANO1/ TMEM16A and K_V4.3 channel compliments have been used to locate these cells directly in coronal sections (Figure 13). Atypical SMCs have an electrophysiological profile unique in smooth muscle physiology, spontaneously firing inward currents that may well be responsible for the STD discharge underlying pacemaker generation in the intact renal pelvis (Figure 13). In contrast, α-SMA$^-$ ICs can be distinguished and located by their expression of ANO1/ TMEM16A and K_V7.5 channel subunits. These markers may well prove invaluable in examining the remodelling of the renal pelvis during hydronephrotic conditions arising after pelviureteric, ureteric or bladder inflow or outflow obstruction.

Acknowledgements

This work was supported in part by the National Health & Medical Research Council (Australia) to RJL and Grant-in-Aids from Japan Society for the Promotion of Science to HH (No.19390418).

Conflicts of interest

The authors declare no conflicting interests.

References

van der Aa F, Roskams T, Blyweert W, Ost D, Bogaert G, De Ridder D (2004). Identification of kit positive cells in the human urinary tract. J Urol 171: 2492–2496.

Albert AP, Pucovsky V, Prestwick SA, Large WA (2006). TRPC3 properties of a native constitutively active Ca^{2+}-permeable cation channel in rabbit ear artey myocytes. J Physiol 571: 361–369.

Alexander SP, Mathie A, Peters JA (2011). Guide to Receptors and Channels (GRAC), 5th edition. Br J Pharmacol 164 (Suppl. 1): S1–S324.

Anderson UA, Carson C, McCloskey KD (2009). KCNQ currents and their contribution to resting membrane potential and the excitability of interstitial cells of Cajal from the guinea pig bladder. J Urol 182: 330–336.

Arena E, Nicotina PA, Arena S, Romeo C, Zuccarello B, Romeo G (2007). Interstitial cells of Cajal network in primary obstructive megaureter. Pediatr Med Chir 29: 28–31.

Arena F, Nicotina PA, Arena S, Romeo C, Zuccarello B, Romeo G (2007). C-kit positive interstitial cells of Cajal network in primary obstructive megaureter. Minerva Pediatr 59: 7–11.

Arena S, Fazzari C, Arena F, Scuderi MG, Romeo C, Nicotina PA *et al.* (2007). Altered 'active' antireflux mechanism in primary vesico-ureteric reflux: a morphological and manometric study. BJU Int 100: 407–412.

Berridge MJ (2008). Smooth muscle cell calcium activation mechanisms. J Physiol 586: 5047–5061.

Britton FC, Ohya S, Horowitz B, Greenwood IA (2002). Comparison of the properties of CLCA1 generated currents and $I_{Cl(Ca)}$ in murine portal vein smooth muscle cells. J Physiol 539: 107–117.

Caputo A, Caci E, Ferrera L, Pedemonte N, Barsanti C, Sondo E *et al.* (2008). TMEM16A, a membrane protein associated with calcium-dependent chloride channel activity. Science 322: 590–594.

David SG, Cebrian C, Vaughan ED, Herzlinger D (2005). C-kit and ureteral peristalsis. J Urol 173: 292–295.

Dixon JS, Gosling JA (1973). The fine structure of pacemaker cells in the pig renal calices. Anat Rec 175: 139–153.

Dixon JS, Gosling JA (1982). The musculature of the human renal calices, pelvis and upper ureter. J Anat 135: 129–137.

Dwyer L, Rhee P-L, Lowe L, Zheng H, Peri L, Ro S *et al.* (2011). Basally active non-selective cation currents regulate the resting membrane potential in human and monkey colonic smooth muscle. Am J Physiol Gastrointest Liver Physiol 301: 6287–6296. ePub May 12.

Galietta LJ (2009). The TMEM16 protein family: a new class of chloride channels? Biophys J 97: 3047–3053.

Golenhofen K, Hannappel J (1973). Normal spontaneous activity of the pyeloureteral system in the guinea-pig. Pflugers Arch 341: 257–270.

Gomez-Pinilla PJ, Gibbons SJ, Bardsley MR, Lorincz A, Pozo MJ, Pasricha PJ *et al.* (2009). Ano1 is a selective marker of interstitial cells of Cajal in the human and mouse gastrointestinal tract. Am J Physiol Gastrointest Liver Physiol 296: G1370–G1381.

Gosling JA, Dixon JS (1972). Structural evidence in support of an urinary tract pacemaker. Br J Urol 44: 550–560.

Gosling JA, Dixon JS (1974). Species variation in the location of upper urinary tract pacemaker cells. Invest Urol 11: 418–423.

Hashitani H, Lang RJ (2010). Functions of ICC-like cells in the urinary tract and male genital organs. J Cell Mol Med 14: 1199–1211.

Hashitani H, Lang RJ, Mitsui R, Mabuchi Y, Suzuki H (2009). Distinct effects of CGRP on typical and atypical smooth muscle cells involved in generating spontaneous contractions in the mouse renal pelvis. Br J Pharmacol 158: 2030–2045.

Huang F, Rock JR, Harfe BD, Cheng T, Huang X, Jan YN *et al.* (2009). Studies on expression and function of the TMEM16A calcium-activated chloride channel. Proc Natl Acad Sci USA 106: 21413–21418.

Imaizumi Y, Muraki K, Watanabe M (1989). Ionic currents in single smooth muscle cells from the ureter of the guinea-pig. J Physiol 411: 131–159.

Kang HJ, Lee HY, Jin MH, Jeong HJ, Han SW (2009). Decreased interstitial cells of Cajal-like cells, possible cause of congenital refluxing megaureters: Histopathologic differences in refluxing and obstructive megaureters. Urology 74: 318–323.

Klemm MF, Exintaris B, Lang RJ (1999). Identification of the cells underlying pacemaker activity in the guinea- pig upper urinary tract. J Physiol 519: 867–884.

Komuro T (1999). Comparative morphology of interstitial cells of Cajal: ultrastructural characterization. Microsc Res Tech 47: 267–285.

Lang RJ (1989). Identification of the major membrane currents in freshly dispersed single smooth muscle cells of guinea-pig ureter. J Physiol 412: 375–395.

Lang RJ (2010). Role of hyperpolarization-activated cation channels in pyeloureteric peristalsis. Kidney Int 77: 483–485.

Lang RJ, Exintaris B, Teele ME, Harvey J, Klemm MF (1998). Electrical basis of peristalsis in the mammalian upper urinary tract. Clin Exp Pharmacol Physiol 25: 310–321.

Lang RJ, Takano H, Davidson ME, Suzuki H, Klemm MF (2001). Characterization of the spontaneous electrical and contractile activity of smooth muscle cells in the rat upper urinary tract. J Urol 166: 329–334.

Lang RJ, Hashitani H, Tonta MA, Parkington HC, Suzuki H (2007a). Spontaneous electrical and Ca^{2+} signals in typical and atypical smooth muscle cells and interstitial cell of Cajal-like cells of mouse renal pelvis. J Physiol 583: 1049–1068.

Lang RJ, Hashitani H, Tonta MA, Suzuki H, Parkington HC (2007b). Role of Ca^{2+} entry and Ca^{2+} stores in atypical smooth muscle cell autorhythmicity in the mouse renal pelvis. Br J Pharmacol 152: 1248–1259.

Lang RJ, Zoltkowski BZ, Hammer JM, Meeker WF, Wendt I (2007c). Electrical characterization of interstitial cells of Cajal-like cells and smooth muscle cells isolated from the mouse ureteropelvic junction. J Urol 177: 1573–1580.

Lang RJ, Hashitani H, Tonta MA, Bourke JL, Parkington HC, Suzuki H (2010). Spontaneous electrical and Ca^{2+} signals in the mouse renal pelvis that drive pyeloureteric peristalsis. Clin Exp Pharmacol Physiol 37: 509–515.

Leblanc N, Ledoux J, Saleh S, Sanguinetti A, Angermann J, O'Driscoll K *et al.* (2005). Regulation of calcium-activated chloride channels in smooth muscle cells: a complex picture is emerging. Can J Physiol Pharmacol 83: 541–556.

Li J, Qu X, Bertram JF (2009). Endothelial-myofibroblast transition contributes to the early development of diabetic renal interstitial fibrosis in streptozotocin-induced diabetic mice. Am J Pathol 175: 1380–1388.

Mackie AR, Byron KL (2008). Cardiovascular KCNQ (Kv7) potassium channels: physiological regulators and new targets for therapeutic intervention. Mol Pharmacol 74: 1171–1179.

Metzger R, Schuster T, Till H, Stehr M, Franke FE, Dietz HG (2004). Cajal-like cells in the human upper urinary tract. J Urol 172: 769–772.

Metzger R, Schuster T, Till H, Franke FE, Dietz HG (2005). Cajal-like cells in the upper urinary tract: comparative study in various species. Pediatr Surg Int 21: 169–174.

Metzger R, Neugebauer A, Rolle U, Bohlig L, Till H (2008). C-Kit receptor (CD117) in the porcine urinary tract. Pediatr Surg Int 24: 67–76.

Murakumo M, Nonomura K, Yamashita T, Ushiki T, Abe K, Koyanagi T (1997). Structural changes of collagen components and diminution of nerves in congenital ureteropelvic junction obstruction. J Urol 157: 1963–1968.

Pezzone MA, Watkins SC, Alber SM, King WE, de Groat WC, Chancellor MB *et al.* (2003). Identification of c-kit-positive cells in the mouse ureter: the interstitial cells of Cajal of the urinary tract. Am J Physiol Renal Physiol 284: F925–F929.

Schroeder BC, Cheng T, Jan YN, Jan LY (2008). Expression cloning of TMEM16A as a calcium-activated chloride channel subunit. Cell 134: 1019–1029.

Smith RD, Borisova L, Wray S, Burdyga T (2002). Characterisation of the ionic currents in freshly isolated rat ureter smooth muscle cells: evidence for species-dependent currents. Pflugers Arch 445: 444–453.

Solari V, Piotrowska AP, Puri P (2003). Altered expression of interstitial cells of Cajal in congenital ureteropelvic junction obstruction. J Urol 170: 2420–2422.

Thorneloe KS, Nelson MT (2004). Properties of a tonically active sodium permeable current in mouse urinary bladder smooth muscle. Am J Physiol Cell Physiol 286: 1246–1257.

Tsuchida S, Suzuki T (1992). Pacemaker activity of the pelvicalyceal border recorded by an intracellular glass microelectrode. Urol Int 48: 121–124.

Weiss R, Wagner ML, Hoffman BF (1967). Localization of the pacemaker for peristalsis in the intact canine ureter. Invest Urol 5: 42–48.

Yang YD, Cho H, Koo JY, Tak MH, Cho Y, Shim WS *et al.* (2008). TMEM16A confers receptor-activated calcium-dependent chloride conductance. Nature 455: 1210–1215.

Zhang SC, Fedoroff S (1997). Cellular localization of stem cell factor and c-kit receptor in the mouse nervous system. J Neurosci Res 47: 1–15.

Zhu MH, Kim TW, Ro S, Yan W, Ward SM, Koh SD *et al.* (2009). A Ca^{2+}-activated Cl^- conductance in interstitial cells of Cajal linked to slow wave currents and pacemaker activity. J Physiol 587: 4905–4918.

Supporting information

Additional Supporting Information may be found in the online version of this article:

Figure S1 Fluorescence micrographs of the kidney from the eYFP-α-SMA transgenic mouse. This mouse has eYFP coupled to the promoter for the gene controlling the expression of α-SMA. (Ai) Low-magnification (×5) fluorescence micrograph of the intact renal pelvis contracting spontaneously. (Aii) Sequential fluorescent images of the renal pelvis in Video S1 were displayed at time intervals of 100 ms and analysed by means of a spatial temporal map (Aiii) of the line drawn in the first panel of Aii, illustrating that contractions occurred at a frequency of about 20 min^{-1}. (B) Low-magnification fluorescence micrograph of coronal section of the mouse kidney illustrating how the α-SMA^+ renal pelvis (RP) envelops the papilla (P); an α-SMA^+ renal artery is denoted by RA. (Ci–ii) Fluorescence micrographs taken in the distal (Ci) and proximal (Cii) regions of a whole mount preparation of the renal pelvis pinned flat in an organ bath and mounted on our fluorescence microscope. Note that the number of cells and the intensity of fluorescence within each cell increased with

distance from the proximal edge of the renal pelvis. (Di–iii) Higher-magnification micrographs taken from the same coronal section of a renal pelvis, confirming that the number and packing of eYFP-α-SMA$^+$ SMCs increases as the wall thickens with distance from the papilla–pelvic border. (Ciii) Illustrates that a cluster of lightly fluorescent α-SMA$^+$ SMCs were often observed at the papilla–pelvic border. Scale bars: (A) 200 μm; (B) 100 μm; (C) 20 μm; (D) 20 μm.

Figure S2 (A) Anti-Kit (Ai, green) and anti-neuronal (PGP9.5, Aii, Aiii red) staining in whole mount preparations of the mouse renal pelvis (Ai–ii) and guinea pig intestine (positive control, Aiii), illustrating that Kit staining in the renal pelvis was restricted to nerves. (Bi–iii) Illustrates that ANO1/ TMEM16A and α-SMA immunostaining co-localized in the smooth muscle layer particularly well in the distal regions of the rat renal pelvis. Calibration bars: (Ai–ii) 100 μm; (Aiii) 50 μm; (Bi–iii) 20 μm.

Video S1 Video of intact preparations of eYFP-α-SMA$^+$ renal pelvis contracting spontaneously. The papilla and surrounding parenchyma have been removed, and the tissue was bathed in a warmed (37°C) PSS.

Video S2 Typical video of single SMC contractions in the proximal region of the eYFP-α-SMA$^+$ renal pelvis. Whole mount preparations of renal pelvis were pinned flat into our organ bath, urothelium uppermost.